



# Arbitrary-Order Sensitivity Analysis in Wave Propagation Problems Using Hypercomplex Spectral Finite Element Method

Juan D. Navarro,<sup>\*</sup> Juan C. Velasquez-Gonzalez,<sup>†</sup> and Mauricio Aristizabal<sup>‡</sup>

*The University of Texas at San Antonio, San Antonio, Texas 78249*

Gregory Jarmer<sup>§</sup> and Seth S. Kessler<sup>¶</sup>

*Metis Design Corporation, Boston, Massachusetts 02114*

and

Arturo Montoya,<sup>\*\*</sup> Harry R. Millwater,<sup>††</sup> and David Restrepo<sup>‡‡</sup>

*The University of Texas at San Antonio, San Antonio, Texas 78249*

<https://doi.org/10.2514/1.J062834>

Many modern structural health monitoring (SHM) systems use piezoelectric transducers to induce and measure guided waves propagating in structures for structural damage detection. To increase the detection capabilities of SHM systems, gradient-based optimization of sensor placement is frequently necessary. However, available numerical differentiation methods for mechanical wave propagation problems suffer from truncation and subtraction errors and are difficult to extend to high-order sensitivities. This paper addresses these issues by introducing an approach to obtain highly accurate numerical sensitivities of arbitrary order in mechanical wave propagation problems. The hypercomplex time-domain spectral finite element method (ZSFEM) couples the hypercomplex Taylor series expansion method with the time-domain spectral finite element method. We show how ZSFEM can be implemented within the commercial finite element package ABAQUS/Explicit. For verification, we compared the numerical and analytical results of the displacement and its sensitivities with respect to mechanical parameters, geometry, and boundary conditions for a rod subjected to a sudden, distributed axial load. First- and second-order sensitivities were obtained with normalized root mean square deviations below  $4 \times 10^{-3}$ . Mesh convergence analyses revealed that  $p$ -refinement offered better convergence rates than  $h$ -refinement for the outputs and their sensitivities. Also, the sensitivities obtained with ZSFEM were compared with finite differences showing higher accuracy and step-size independence (e.g., no iteration is needed to determine the step size that minimizes the error). For simplicity, ZSFEM was presented only for one-dimensional truss elements, but the method is general and can be applied to other elements.

## I. Introduction

THE assessment of the structural integrity in engineered systems is commonly known as nondestructive evaluation (NDE). Recent developments in NDE systems have investigated the integration of permanent sensors within the structure to monitor its integrity automatically, reducing the need for human intervention. This sub-discipline has been called structural health monitoring (SHM). SHM aims to detect the existence of structural damages, locate the physical position of the damage, and quantify the severity of the damage to facilitate the prognosis of the remaining service life of the structure [1]. Among the different types of SHM systems, guided wave-based SHM systems have gained great interest for several reasons: i) the transducers required are usually lightweight and easy to integrate into the structure; ii) large areas can be scanned with a relatively small number of transducers; and iii) microscale damages can be detected as the transducers are capable of measuring high-frequency

excitations while reducing the sensitivity to low-frequency ambient noise [2–5].

The position of the sensors used in SHM systems can profoundly affect its capacity to detect structural damage. As such, the placement of the transducers in a structure is typically selected based on Bayesian and gradient-based optimization algorithms in digital twins to maximize the detection information while minimizing the number of transducers required [6–11]. Among the optimization algorithms traditionally used for sensor placement, one can find the conjugate gradient, least-squares regression using bidiagonalization and QR decomposition, and the Broyden–Fletcher–Goldfarb–Shanno (BFGS). All of these algorithms use the information from sensitivities to guide the optimization process [12,13]. Because the objective function used in optimizing sensor placement is expensive to evaluate, highly accurate sensitivities are desired to minimize the computational cost of the optimization process [14]. Moreover, access to highly accurate sensitivities leads to improved guided wave-based SHM systems by maximizing their sensitivity to microscale damage, different types of imperfections, noise in measurements, and changes in environmental conditions [15–17]. Therefore, advances in differentiation techniques in the computational simulation of mechanical wave propagation problems are required to accelerate and facilitate optimization processes necessary in SHM.

Mechanical wave propagation problems are typically simulated using explicit time integration algorithms [2,18]. Different methods can be used to calculate the sensitivities required to guide optimization processes within the framework of explicit solvers [14]. The finite difference method (FDM) is the most traditional approach to computing numerical sensitivities thanks to the simplicity of its implementation [19,20]. However, the accuracy of FDM is prone to truncation and subtraction error [21], and determining the optimal perturbation step magnitude that minimizes both errors is a nontrivial problem that requires multiple iterations [22–24]. This fundamental obstacle becomes more relevant when computing higher-order

Received 20 January 2023; revision received 8 November 2023; accepted for publication 4 December 2023; published online Open Access 18 January 2024. Copyright © 2024 by the American Institute of Aeronautics and Astronautics, Inc. All rights reserved. All requests for copying and permission to reprint should be submitted to CCC at [www.copyright.com](http://www.copyright.com); employ the eISSN 1533-385X to initiate your request. See also AIAA Rights and Permissions [www.aiaa.org/randp](http://www.aiaa.org/randp).

<sup>\*</sup>Ph.D. Candidate, Department of Mechanical Engineering.

<sup>†</sup>Ph.D. Student, Department of Mechanical Engineering.

<sup>‡</sup>Post-Doctoral Scholar, Department of Mechanical Engineering.

<sup>§</sup>R&D Engineer, Metis Design Corporation.

<sup>¶</sup>President/CEO, Metis Design Corporation.

<sup>\*\*</sup>Associate Professor, Department of Mechanical Engineering and School of Civil & Environmental Engineering, and Construction Management.

<sup>††</sup>Samuel G. Dawson Endowed Professor, Associate Chair for Research, Department of Mechanical Engineering.

<sup>‡‡</sup>Assistant Professor, Department of Mechanical Engineering; david.restrepo@utsa.edu (Corresponding Author).

sensitivities [14]. The adjoint variable method (AVM) has also been used to compute numerical sensitivities in mechanical wave propagation problems. However, AVM requires the development of an adjoint system of equations, leading to significant increase in computational cost to compute the required sensitivities [12]. Also, AVM is known for its difficulties to extend to higher-order sensitivities [25]. Recently, algorithmic differentiation (AD) has been gaining popularity; however, AD requires access to source code and code conversion packages specific to the programming language being used [26–28]. In addition, higher-order sensitivities are prohibitively expensive to compute with AD [29].

An alternative method to obtain highly accurate sensitivities was introduced by Squire and Trapp [30], based on using complex variables to approximate the sensitivities of real functions. Like FDM, this method adds a small perturbation to the function of interest; however, the perturbation takes place in an imaginary direction instead of a real axis. Then, the sensitivity is obtained by truncating an infinite Taylor series expansion of the complex function. This method is known as the complex Taylor series expansion (CTSE). CTSE is not susceptible to the subtractive errors that are characteristic of FDM because there is no subtraction of similar quantities [31]. Nonetheless, CTSE is only valid for first-order sensitivities. Lantoine et al. [32] addressed this issue by including multicomplex numbers, allowing one to compute arbitrary-order sensitivities with high accuracy. This extension of CTSE is known as the multicomplex Taylor series expansion due to the inclusion of multiple imaginary axes. In parallel, Fike and Alonso [33] introduced the use of dual [34] and hyper-dual numbers to obtain calculations of second-order sensitivities with machine precision. These methods are known as the hypercomplex Taylor series expansion (ZTSE). Sensitivities computed with multicomplex numbers require using a small perturbation step (i.e.,  $10^{-10}$ ) to reduce the truncation error below the machine precision, causing numerical issues in linear algebra operations of matrices containing quantities that are orders of magnitude different. In contrast, with hyper-dual numbers the computation of sensitivities has machine precision accuracy regardless on the selection of the perturbation step. Moreover, complex algebra requires higher number of calculations than its dual algebra counterpart, resulting in a performance improvement when dual algebra is used [35,36]. For these reasons, in this work we use hyper-dual numbers with unitary perturbation steps.

ZTSE as differentiation method is agnostic to the solution method used to model problem of interest. Specifically, in wave propagation problems both analytical [37,38] and numerical [39] methods can be benefited from leveraging ZTSE for sensitivity analysis. Recently, ZTSE was coupled with the finite element method (FEM) giving rise to the hypercomplex finite element method (ZFEM) [40,41]. ZFEM inherits FEM's flexibility to model complex geometrical configurations while preserving high accuracy. Moreover, with ZFEM it is possible to compute arbitrary-order sensitivities with high accuracy in a single FEM run. The tradeoffs are that ZFEM is intrusive as it requires the implementation of hypercomplex operations, and the size of the system of equations grows with the order of the sensitivities. Recently, ZTSE and ZFEM have been used to perform sensitivity analysis in a large variety of disciplines, such as computational fluid dynamics [42–45], pseudospectral algorithms [46], aeroelasticity [47], chemical reactions [48], gradient-based optimization [49], boundary elements [50], structural dynamics [51–55], phononics [56], nonlinear analyses [57,58], frictional contact [59], thermoelasticity [60–63], fatigue [64], plasticity [65], creep [66], bioheat transfer [67], residual stress [68], and fracture mechanics [69]. Despite the numerous advantages of ZFEM, its application in time-domain mechanical wave propagation problems is still absent.

FEM is known to be an effective numerical tool for the solution of boundary value problems on arbitrary and complex domains. However, the standard formulation for FEM is not appropriate for solving mechanical wave propagation problems [70] as the detection of small damage features requires high-frequency excitation signals. Thus, the precise computational representation of these problems using FEM requires very dense spatial and time discretization, result-

ing in high computational costs [71]. Spectral finite element method (SFEM) has been proposed to address this issue [72–75]. Although the formulation of SFEM is very similar to that of FEM; SFEM uses an interpolating polynomial of high degree based on the Gauss–Lobatto–Legendre (GLL) quadrature, and it places the nodes and the integration points at the same positions. High-order shape functions and nodal quadrature make the simulation of time domain wave propagation problems accurate and fast compared to standard FEM [75–78].

In this work, we introduce a new method to obtain highly accurate, arbitrary-order sensitivities in the simulation of time domain mechanical wave propagation problems by coupling ZTSE with the time-domain spectral finite element method (SFEM) herein called the time-domain hypercomplex time-domain spectral finite element method (ZSFEM). ZSFEM can accurately model mechanical wave propagation phenomena and simultaneously provide arbitrary-order sensitivities without dependency on the selection of perturbation steps. The outline for the rest of this work is as follows: Sec. II provides the background information about computing arbitrary-order sensitivities with ZTSE. Section III presents the new methodology and the implementation aspects of ZSFEM. Then, in Sec. IV, an application study based on the sensitivity analysis of a rod subjected to harmonic axial load is presented. Finally, the conclusions and future work are presented in Sec. V.

## II. Arbitrary-Order Differentiation with the Hypercomplex Taylor Series Expansion

ZTSE is a numerical method that uses dual numbers to compute sensitivities with high accuracy [33]. Dual numbers [hereafter represented with an asterisk superscript (\*)] are a subset of the set of hypercomplex numbers [79]. ZTSE obtains the sensitivity of a function  $f(x)$  by adding a perturbation  $h$  to the variable of interest  $x$  along a nonreal axis  $\epsilon_1$ , becoming  $x^* = x + h\epsilon_1$ , and evaluating the Taylor series expansion of the function at the perturbed position:

$$f(x + h\epsilon_1) = f(x) + \frac{h\epsilon_1}{1!} \frac{df(x)}{dx} + \frac{(h\epsilon_1)^2}{2!} \frac{d^2f(x)}{dx^2} + \frac{(h\epsilon_1)^3}{3!} \frac{d^3f(x)}{dx^3} + \frac{(h\epsilon_1)^4}{4!} \frac{d^4f(x)}{dx^4} + \dots \quad (1)$$

Considering the properties of dual numbers,  $\epsilon_1^2 = 0$  and  $\epsilon_1 \neq 0$ , the higher-order terms in the right-hand side of Eq. (1) can be eliminated [80]. Therefore, the first-order sensitivity can be exactly computed by taking the dual imaginary part of both sides of Eq. (1) as

$$\frac{df(x)}{dx} = \frac{Im_{\epsilon_1}[f(x + h\epsilon_1)]}{h} \quad (2)$$

where  $Im_{\epsilon_1}[\cdot]$  denotes the nonreal part of the dual number corresponding to the axis  $\epsilon_1$ . Note that the Taylor series expansion in Eq. (1) was not truncated; hence, ZTSE is exact and insensitive to the selection of the perturbation step  $h$ . In general, a unitary step size  $h = 1$  is used for simplicity and omitted in the expressions presented hereafter.

ZTSE can compute higher-order sensitivities by introducing additional nonreal axes using hyper-dual numbers. Hyper-dual numbers are the generalization of dual numbers to higher dimensions [81]. To compute  $n$  th-order sensitivities with ZTSE, it is necessary to use hyper-dual numbers with  $2^n - 1$  nonreal axes. For instance, to obtain second-order sensitivities it is necessary to use three nonreal axes (e.g.,  $\epsilon_1, \epsilon_2$ , and  $\epsilon_{12}$ ), where the first two are independent and the third one is a mixed axis. In general, the highest-order sensitivity to be computed determines the number of independent nonreal axes perturbed, which means that to compute the  $n$  th-order sensitivity of  $f(x)$  will require a hyper-dual number with unitary perturbations along  $n$  independent nonreal axes  $f(x + \epsilon_1 + \epsilon_2 + \dots + \epsilon_n)$ . Thereafter, the general expression for arbitrary-order sensitivities with ZTSE is as follows:

$$\frac{\partial^n f(x)}{\partial x^n} = Im_{\epsilon_1 \dots \epsilon_n} \left[ f \left( x + \sum_{j=1}^n \epsilon_j \right) \right] \quad (3)$$

In the case of mixed sensitivities, each variable is perturbed along different nonreal axes. For instance, a  $n$  th-order mixed sensitivity of a function  $f(x_1, x_2, \dots, x_m)$  with  $m$  input parameters will require a hyper-dual number with unitary perturbations along different  $n$  non-real axes, as shown in Eq. (4) [82].

$$\frac{\partial^n f(x_1, x_2, \dots, x_m)}{\partial x_1^{b_1} \partial x_2^{b_2} \dots \partial x_m^{b_m}} = Im_{\epsilon_1 \dots \epsilon_n} \left[ f \left( x_1 + \sum_{j_1=1}^{b_1} \epsilon_{j_1}, x_2 + \sum_{j_2=b_1+1}^{b_1+b_2} \epsilon_{j_2}, \dots, x_m + \sum_{j_m=b_{m-1}+1}^{b_1+b_2+\dots+b_m} \epsilon_{j_m} \right) \right] \quad (4)$$

where  $\sum_{j=1}^m b_j = n$ . An important advantage of ZTSE is given by the possibility of computing the real-valued analysis and its corresponding sensitivities simultaneously in a single analysis, including lower-order (e.g.,  $< n$ ) sensitivities when computing  $n$  th-order sensitivities. For instance, when the second-order mixed sensitivity  $\partial^2 f(x_1, x_2)/\partial x_1 \partial x_2$  is computed, the first-order sensitivities  $\partial f(x_1, x_2)/\partial x_1$  and  $\partial f(x_1, x_2)/\partial x_2$  and the real-valued result are obtained in the same analysis, as shown below:

$$\begin{aligned} f(x, y) &= \text{Real}[f(x_1 + \epsilon_1, x_2 + \epsilon_2)] \\ \frac{\partial f(x_1, x_2)}{\partial x_1} &= Im_{\epsilon_1}[f(x_1 + \epsilon_1, x_2 + \epsilon_2)] \\ \frac{\partial f(x_1, x_2)}{\partial x_2} &= Im_{\epsilon_2}[f(x_1 + \epsilon_1, x_2 + \epsilon_2)] \\ \frac{\partial^2 f(x_1, x_2)}{\partial x_1 \partial x_2} &= Im_{\epsilon_{12}}[f(x_1 + \epsilon_1, x_2 + \epsilon_2)] \end{aligned} \quad (5)$$

where the Taylor series expansion of  $f(x_1 + \epsilon_1, x_2 + \epsilon_2)$  is given by

$$\begin{aligned} f(x_1 + \epsilon_1, x_2 + \epsilon_2) &= f(x_1, x_2) + \frac{\epsilon_1}{1!} \frac{\partial f(x_1, x_2)}{\partial x_1} \\ &+ \frac{\epsilon_2}{1!} \frac{\partial f(x_1, x_2)}{\partial x_2} + \frac{\epsilon_{12}}{1!} \frac{\partial^2 f(x_1, x_2)}{\partial x_1 \partial x_2} \end{aligned} \quad (6)$$

Note that the first term on the right-hand side corresponds to the evaluation of the function  $f(x_1, x_2)$  stored in the real part of the solution; the second and the third terms correspond to the first-order sensitivities, each one stored in independent nonreal axes  $\epsilon_1$  and  $\epsilon_2$ , respectively; and the fourth term corresponds to the second-order sensitivity stored in the mixed nonreal axis  $\epsilon_{12}$ .

There are two alternatives to operate hyper-dual variables in traditional programming languages that do not support hypercomplex algebras: one alternative is to use the Cauchy–Riemann (CR) matrix notation of hyper-dual numbers (see the Appendix for more information about CR notation). This matrix notation allows one to replace hyper-dual numbers with matrices containing real-valued numbers, and the hyper-dual operations are replaced by matrix operations [69,80,83–88]. Although CR flexibility allows one to implement hyper-dual algebra in real-valued programming languages, the incurred computational cost is significant as CR increases the size of the variables by a factor of  $4^n$  to compute an  $n$ th-order sensitivity. This results in a significant increase in memory consumption and the number of operations. The other alternative is to use external libraries that support operations involving hyper-dual numbers. External libraries use operator overloading to operate hyper-dual numbers and only increase the size of the variables by a factor of  $2^n$ . In this study the FORTRAN external library MultiZ was used as presented in the work of Aguirre-Mesa et al. [83].

### III. Hypercomplex Spectral Finite Element Method

The ZSFEM can model mechanical wave propagation phenomena and simultaneously provide arbitrary-order sensitivities with high accuracy of the model outputs with respect to the inputs, e.g., mechanical parameters, geometry, and boundary conditions. An overview of ZSFEM is presented in Fig. 1, where the inputs of the method correspond to the highest order of sensitivity to compute,  $n$ , and the set of input parameters describing the wave propagation model,  $\alpha = \{\alpha_1, \alpha_2, \dots\}$ . The method requires a single-time code modification in step 0 corresponding to setting all the input parameters into their hyper-dual representation. From this point onward, the method is divided into preprocessing, processing, and postprocessing. Preprocessing covers step 1 and corresponds to setting the perturbation to the variables whose sensitivities will be calculated. Processing covers steps 2 and 3 and corresponds to the domain discretization using SFEM and the solution of the equations of motion in the time domain; these steps were implemented in Abaqus/Explicit as a VUEL subroutine. Postprocessing covers step 4 and corresponds to the extraction of the model outputs and the sensitivity information. Each step of the methodology is described below:

0) Step zero consists of representing each input parameter as hyper-dual variables  $\alpha^* = \{\alpha_1^*, \alpha_2^*, \dots\}$ . This step is a one-time modification that is performed by declaring the input variables as hyper-dual variables.

1) In the first step, unitary perturbations are added to the nonreal axes of the variables of interest. The maximum order of derivative to compute  $n$  determines the number of independent nonreal axes to be perturbed. Adding perturbations to the *same* parameter along different independent nonreal axes  $\alpha_i^* = \alpha_i^{Re} + \epsilon_1 + \dots + \epsilon_n$  will result in the computation of sensitivities with respect to the perturbed

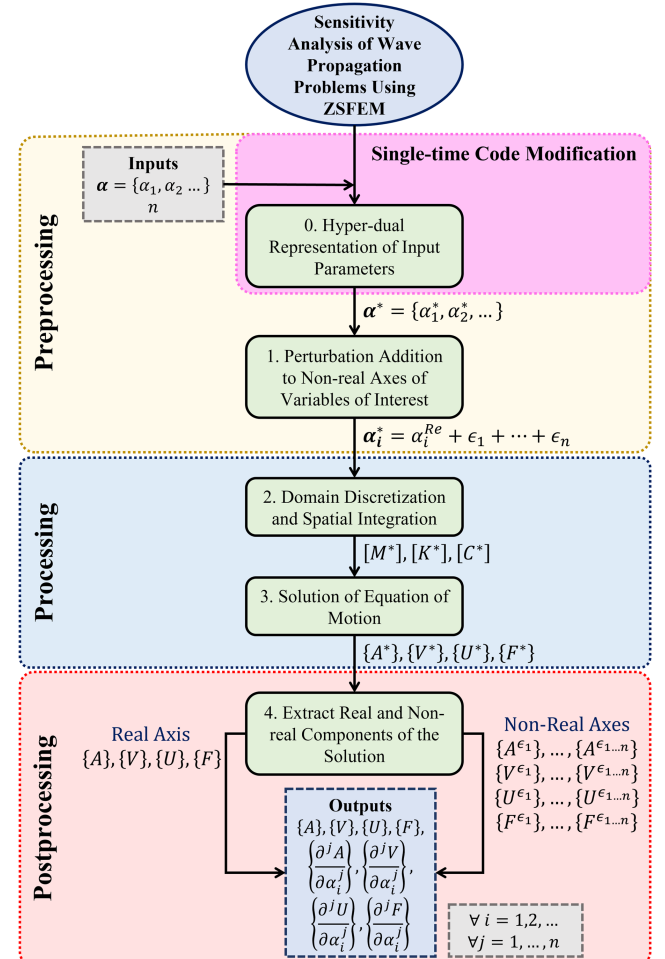


Fig. 1 Methodology flowchart for sensitivity analysis in wave propagation problems using ZSFEM.

parameter. On the other hand, perturbing multiple parameters along *different* independent nonreal axes  $\alpha_i^* = \alpha_i^{Re} + \epsilon_i$  will result in the computation of mixed sensitivities.

2) In the second step of the method, the elements' mass  $[M^*]$  and stiffness  $[K^*]$  matrices are computed using traditional SFEM formulations (see [70,73,75]). As such, the discretization and integration algorithms traditionally used in SFEM are unchanged; however, as the variables are hyper-dual, algebraic operations are conducted using the MultiZ library.

The elements' damping matrix is computed using Rayleigh proportional damping as a linear combination of the mass and stiffness matrices:

$$[C] = C_\alpha[M] + C_\beta[K] \quad (7)$$

where  $C_\alpha$  and  $C_\beta$  are the Rayleigh proportional damping coefficients of the mass and stiffness matrices, respectively. To compute sensitivities with respect these parameters, we define the hyper-dual damping matrix based on the real part of the mass and stiffness matrices and the hyper-dual Rayleigh proportional damping coefficients:

$$[C^*] = C_\alpha^*[M^{Re}] + C_\beta^*[K^{Re}] \quad (8)$$

3) The wave propagation phenomenon is modeled by solving the time-domain equation of motion:

$$[M^*]\{A^*\} + [C^*]\{V^*\} + [K^*]\{U^*\} = \{F^*\} \quad (9)$$

where  $[M^*]$ ,  $[C^*]$ , and  $[K^*]$  are the mass, damping, and stiffness matrices, and  $\{A^*\}$ ,  $\{V^*\}$ ,  $\{U^*\}$ , and  $\{F^*\}$  are the nodal accelerations, velocities, displacements, and external forces, respectively. In the context of transient dynamic simulations, widely used commercial FEM packages such as ABAQUS/Explicit and ANSYS/LS-Dyna employ the central difference method (CDM) as time-stepping algorithm [71,89,90]. CDM is a second-order-accurate explicit method that approximates the time derivatives of the equation of motion. It advances in time by solving Eq. (9) to obtain the nodal accelerations:

$$\{A^*\} = [M^*]^{-1} \{ \{F^*\} - [C^*]\{V^*\} - [K^*]\{U^*\} \} \quad (10)$$

CDM is known to be conditionally stable. To ensure the stability of CDM, a widely employed approach is to impose the Courant–Friedrichs–Lewy (CFL) condition. CFL provides a constraint on the time step size, preventing the growth of numerical instabilities arising from time discretization errors. In the context of explicit time integration schemes, the CFL condition states that the time step size must be chosen small enough so that the wave propagates only a fraction of the grid size during each time-step. This ensures that the numerical solution remains stable and accurately captures the dynamics of the system. The CFL equation for determining the appropriate time increment can be expressed as

$$\Delta t = \text{CFL} \frac{d_{\min}}{c} \quad (11)$$

where  $d_{\min}$  is the shortest distance between any nodes in the mesh of elements and  $c = \sqrt{E/\rho}$  is the wave velocity. From steps 0–2, all the variables involved in Eq. (10) are hyper-dual of order  $n$ . Therefore, to take advantage of existing open source or commercial CDM solvers, it is necessary to consider some methodological modifications. Following Millwater et al. [91,92], any hyper-dual element can be represented as a traditional SFEM element with additional sets of nodes that carry the information of the nonreal axes. For example, Fig. 2 shows a schematic of a 2D element used in SFEM compared with a ZSFEM element for computing second-order sensitivities. In this case, ZSFEM requires three additional sets of nodes for each real node corresponding to the nonreal axes  $\epsilon_1$ ,  $\epsilon_2$ , and  $\epsilon_{12}$ .

Following the representation for ZSFEM introduced by Millwater et al. [91,92], Eq. (10) is rewritten using CR notation. (For reference,

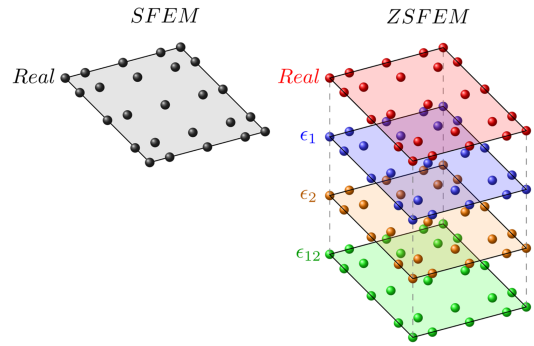


**Fig. 2** Comparison of 2D elements used in SFEM and ZSFEM when computing second-order sensitivities.

the CR form to represent any hyper-dual number is presented in the Appendix.) It is important to highlight that MultiZ is used to operate all the hyper-dual input parameters  $\alpha^*$  to compute  $[M^*]$ ,  $[K^*]$ , and  $[C^*]$  in step 3 and that CR notation is only used as a resource to solve the equation of motion in real-valued solvers (e.g., Abaqus, Ansys, and others). The resulting system of equations (SOEs) has the following form:

$$\begin{pmatrix} \{A^{Re}\} \\ \{A^{\epsilon_1}\} \\ \vdots \\ \{A^{\epsilon_{12\dots n-1}}\} \\ \{A^{\epsilon_{12\dots n}}\} \end{pmatrix} = \begin{bmatrix} [M^{Re}] & 0 & \dots & 0 & 0 \\ [M^{\epsilon_1}] & [M^{Re}] & \dots & 0 & 0 \\ \vdots & \vdots & \ddots & \vdots & \vdots \\ [M^{\epsilon_{12\dots n-1}}] & 0 & \dots & [M^{Re}] & 0 \\ [M^{\epsilon_{12\dots n}}] & [M^{\epsilon_{12\dots n-1}}] & \dots & [M^{\epsilon_1}] & [M^{Re}] \end{bmatrix}^{-1} \\ \times \begin{pmatrix} \{F^{Re}\} \\ \{F^{\epsilon_1}\} \\ \vdots \\ \{F^{\epsilon_{12\dots n-1}}\} \\ \{F^{\epsilon_{12\dots n}}\} \end{pmatrix} - \begin{bmatrix} [C^{Re}] & 0 & \dots & 0 & 0 \\ [C^{\epsilon_1}] & [C^{Re}] & \dots & 0 & 0 \\ \vdots & \vdots & \ddots & \vdots & \vdots \\ [C^{\epsilon_{12\dots n-1}}] & 0 & \dots & [C^{Re}] & 0 \\ [C^{\epsilon_{12\dots n}}] & [C^{\epsilon_{12\dots n-1}}] & \dots & [C^{\epsilon_1}] & [C^{Re}] \end{bmatrix} \\ \times \begin{pmatrix} \{V^{Re}\} \\ \{V^{\epsilon_1}\} \\ \vdots \\ \{V^{\epsilon_{12\dots n-1}}\} \\ \{V^{\epsilon_{12\dots n}}\} \end{pmatrix} - \begin{bmatrix} [K^{Re}] & 0 & \dots & 0 & 0 \\ [K^{\epsilon_1}] & [K^{Re}] & \dots & 0 & 0 \\ \vdots & \vdots & \ddots & \vdots & \vdots \\ [K^{\epsilon_{12\dots n-1}}] & 0 & \dots & [K^{Re}] & 0 \\ [K^{\epsilon_{12\dots n}}] & [K^{\epsilon_{12\dots n-1}}] & \dots & [K^{\epsilon_1}] & [K^{Re}] \end{bmatrix} \\ \times \begin{pmatrix} \{U^{Re}\} \\ \{U^{\epsilon_1}\} \\ \vdots \\ \{U^{\epsilon_{12\dots n-1}}\} \\ \{U^{\epsilon_{12\dots n}}\} \end{pmatrix} \quad (12)$$

To note, all the variables in Eq. (12) are real. The superscripts  $(\cdot)^{Re}$ ,  $(\cdot)^{\epsilon_1}$ ,  $(\cdot)^{\epsilon_{n-1}}$ , and  $(\cdot)^{\epsilon_n}$  denote the real part of the hypercomplex variable and the nonreal parts corresponding to the  $\epsilon_1$ ,  $\epsilon_{12\dots n-1}$ , and  $\epsilon_{12\dots n}$  axes, respectively. However, in this representation of the equation of motion, the mass matrix is not diagonal and evaluating its inverse in a CDM scheme becomes computationally expensive. To address this point, we present a procedure that uncouples the system of equations by solving each equation individually. In the case of the first equation, only the real part of the variables is required, and the solution for the acceleration is found:

$$\{A^{Re}\} = [M^{Re}]^{-1} \{ \{F^{Re}\} - [C^{Re}]\{V^{Re}\} - [K^{Re}]\{U^{Re}\} \} \quad (13)$$

Equation (13) requires inverting  $[M^{Re}]$ , which by construction with SFEM is diagonal [77,93,94]. This characteristic feature of SFEM is preserved in other types of elements, such as 2D plane and 3D brick elements with arbitrary shapes. Then, the solution of the real part of the acceleration is used to compute the second row of the SOE in Eq. (12), which corresponds to the first nonreal part of the acceleration:

$$\{A^{\epsilon_1}\} = [M^{Re}]^{-1}(\{F^{\epsilon_1}\} - [C^{\epsilon_1}]\{V^{Re}\} - [C^{Re}]\{V^{\epsilon_1}\} - [K^{\epsilon_1}]\{U^{Re}\} - [K^{Re}]\{U^{\epsilon_1}\} - [M^{\epsilon_1}]\{A^{Re}\}) \quad (14)$$

In general, the solution of the  $n$ th nonreal part of the acceleration only depends on the information of the real part of the acceleration and all the lower order ( $< n$ ) nonreal parts of the acceleration:

$$\{A^{\epsilon_{12\dots n}}\} = [M^{Re}]^{-1}(\{F^{\epsilon_{12\dots n}}\} - [C^{\epsilon_{12\dots n}}]\{V^{Re}\} - [C^{\epsilon_{12\dots n-1}}]\{V^{\epsilon_1}\} - \dots - [C^{\epsilon_1}]\{V^{\epsilon_{12\dots n-1}}\} - [C^{Re}]\{V^{\epsilon_{12\dots n}}\} - [K^{\epsilon_{12\dots n}}]\{U^{Re}\} - [K^{\epsilon_{12\dots n-1}}]\{U^{\epsilon_1}\} - \dots - [K^{\epsilon_1}]\{U^{\epsilon_{12\dots n-1}}\} - [K^{Re}]\{U^{\epsilon_{12\dots n}}\} - [M^{\epsilon_{12\dots n}}]\{A^{Re}\} - [M^{\epsilon_{12\dots n-1}}]\{A^{\epsilon_1}\} - \dots - [M^{\epsilon_1}]\{A^{\epsilon_{12\dots n-1}}\}) \quad (15)$$

The CDM advances in time and finds the time-dependent solution vectors ( $\{U^*\}, \{V^*\}, \{A^*\}, \{F^*\}$ ). Here, any real-only CDM solver can be used; i.e., no hypercomplex-valued CDM solver is required.

4) Lastly, in the fourth step, the real and nonreal components of the solution vectors ( $\{U\}, \{V\}, \{A\}, \{F\}$ ) are separated. The real components correspond to the solution of the nominal problem, and the information of the sensitivities is contained in the nonreal axes of the solution vectors and postprocessed using Eqs. (3) and (4). For simplicity, we show the case of the nodal displacements, but the expressions are also valid for the remaining solution vectors ( $\{V\}, \{A\}, \{F\}$ ). Assume that variable  $\alpha_i$  is perturbed along  $\epsilon_i$ :

First order:

$$\frac{\partial\{U^*\}}{\partial\alpha_1} = Im_{\epsilon_1}[\{U^*\}] = \{U^{\epsilon_1}\}, \frac{\partial\{U^*\}}{\partial\alpha_2} = Im_{\epsilon_2}[\{U^*\}] = \{U^{\epsilon_2}\}, \dots, \frac{\partial\{U^*\}}{\partial\alpha_n} = Im_{\epsilon_n}[\{U^*\}] = \{U^{\epsilon_n}\}$$

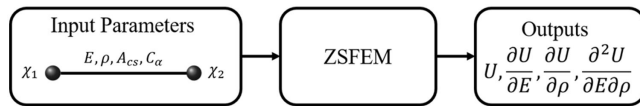
Second order:

$$\frac{\partial^2\{U^*\}}{\partial\alpha_1\partial\alpha_2} = Im_{\epsilon_{12}}[\{U^*\}] = \{U^{\epsilon_{12}}\}, \dots, \frac{\partial^2\{U^*\}}{\partial\alpha_1\partial\alpha_n} = Im_{\epsilon_{1n}}[\{U^*\}] = \{U^{\epsilon_{1n}}\}$$

Third order:

$$\frac{\partial^3\{U^*\}}{\partial\alpha_1\partial\alpha_2\partial\alpha_3} = Im_{\epsilon_{123}}[\{U^*\}] = \{U^{\epsilon_{123}}\}, \dots, \frac{\partial^3\{U^*\}}{\partial\alpha_1\partial\alpha_2\partial\alpha_n} = Im_{\epsilon_{12n}}[\{U^*\}] = \{U^{\epsilon_{12n}}\}$$

$$\vdots$$



a)

$n$ th order:

$$\frac{\partial^n\{U^*\}}{\prod_{j=1}^n \partial\alpha_j} = Im_{\epsilon_{12\dots n}}[\{U^*\}] = \{U^{\epsilon_{12\dots n}}\} \quad (16)$$

### A. Step-by-Step Application Example

To illustrate the new methodology for computing arbitrary-order sensitivities in mechanical wave propagation problems using ZSFEM, we present a step-by-step analysis of a single linear spectral truss element with Young's modulus  $E$ , density  $\rho$ , cross-sectional area  $A_{cs}$ , Rayleigh proportional parameters  $C_\alpha$  and  $C_\beta$ , and nodal coordinates  $\chi_1$  and  $\chi_2$ . The objective in this example is to compute the mixed second-order sensitivity of the nodal displacements with respect to the Young's modulus  $E$  and the density  $\rho$ , as shown in Fig. 3a.

Follow the steps listed in the flowchart shown in Fig. 1:

0) For the case of mixed second-order sensitivities, all the input parameters are represented as hyper-dual variables with order 2 and 3 nonreal axes  $\epsilon_1, \epsilon_2$  and  $\epsilon_{12}$ :

$$\alpha^* = \{E^*, \rho^*, A_{cs}^*, \chi_1^*, \chi_2^*, C_\alpha^*, C_\beta^*\} \quad (17)$$

1) Unitary perturbations are added to the variables of interest  $E$  and  $\rho$  along two independent nonreal axes  $\epsilon_1$  and  $\epsilon_2$ , respectively, as shown in Fig. 3:

$$E^* = E^{Re} + \epsilon_1$$

$$\rho^* = \rho^{Re} + \epsilon_2 \quad (18)$$

2) Figure 3b shows a schematic representation for a bi-dual truss element with a unitary perturbation on the Young's modulus along  $\epsilon_1$  and another unitary perturbation on the density along  $\epsilon_2$ . Note also that the nonreal values of the remaining input parameters (i.e., nodal coordinates  $\chi_1$  and  $\chi_2$ , cross-sectional area  $A_{cs}$ , and Rayleigh proportional damping parameters  $C_\alpha$  and  $C_\beta$ ) are set to zero. The element's mass, stiffness, and damping matrices are computed as follows:

$$[M^*] \approx \sum_{i=1}^{p+1} w_i [\psi(\xi_i)]^T \rho^* A_{cs} [\psi(\xi_i)] \det([J(\chi^*, \xi_i)])$$

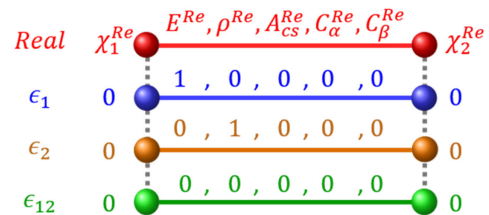
$$\approx \frac{A_{cs}(\rho^{Re} + \epsilon_2)(\chi_2 - \chi_1)}{2} \begin{bmatrix} 1 & 0 \\ 0 & 1 \end{bmatrix}$$

$$[K^*] \approx \sum_{i=1}^{p+1} w_i [B(\chi^*, \xi_i)]^T E^* A_{cs} [B(\chi^*, \xi_i)] \det([J(\chi^*, \xi_i)])$$

$$\approx \frac{A_{cs}(E^{Re} + \epsilon_1)}{\chi_2 - \chi_1} \begin{bmatrix} 1 & -1 \\ -1 & 1 \end{bmatrix}$$

$$[C^*] \approx C_\alpha^* [M^{Re}] + C_\beta^* [K^{Re}] \approx \frac{A_{cs} C_\alpha^{Re} \rho^{Re} (\chi_2 - \chi_1)}{2} \begin{bmatrix} 1 & 0 \\ 0 & 1 \end{bmatrix}$$

$$+ \frac{A_{cs} E^{Re} C_\beta^{Re}}{\chi_2 - \chi_1} \begin{bmatrix} 1 & -1 \\ -1 & 1 \end{bmatrix} \quad (19)$$



b)

Fig. 3 a) Schematic for second-order sensitivity computation in linear truss element using ZSFEM. b) Bi-dual linear truss element with perturbations on Young's modulus and density.

where  $\xi_i$  are the nodal coordinates of the  $i$ th node in the isoparametric space and  $J$  is the jacobian that maps the nodal coordinate from the physical space ( $\chi^*$ ) into the isoparametric space.

3) The SOE is reorganized in order to solve the equation of motion. For reference, the matrices for this example are presented in the Appendix. The solution of the real part [the first line of the SOE shown in Eq. (12)] corresponds to

$$\begin{Bmatrix} A_1^{Re} \\ A_2^{Re} \end{Bmatrix} = [M^{Re}]^{-1} \left\{ \begin{Bmatrix} F_1^{Re} \\ F_2^{Re} \end{Bmatrix} - [C^{Re}] \begin{Bmatrix} V_1^{Re} \\ V_2^{Re} \end{Bmatrix} - [K^{Re}] \begin{Bmatrix} U_1^{Re} \\ U_2^{Re} \end{Bmatrix} \right\} \quad (20)$$

Then, the first nonreal part of the acceleration vector [the second line of the SOE shown in Eq. (12)] is computed using Eq. (14). In this application example,  $[M^{\epsilon_1}]$  and  $[C^{\epsilon_1}]$  are zero, yielding to the following expression:

$$\begin{Bmatrix} A_1^{\epsilon_1} \\ A_2^{\epsilon_1} \end{Bmatrix} = [M^{Re}]^{-1} \left\{ \begin{Bmatrix} F_1^{\epsilon_1} \\ F_2^{\epsilon_1} \end{Bmatrix} - [C^{\epsilon_1}] \begin{Bmatrix} V_1^{Re} \\ V_2^{Re} \end{Bmatrix} - [C^{Re}] \begin{Bmatrix} V_1^{\epsilon_1} \\ V_2^{\epsilon_1} \end{Bmatrix} - [K^{\epsilon_1}] \begin{Bmatrix} U_1^{Re} \\ U_2^{Re} \end{Bmatrix} - [K^{Re}] \begin{Bmatrix} U_1^{\epsilon_1} \\ U_2^{\epsilon_1} \end{Bmatrix} - [M^{\epsilon_1}] \begin{Bmatrix} A_1^{Re} \\ A_2^{Re} \end{Bmatrix} \right\} \quad (21)$$

The second nonreal part of the acceleration vector [the third line of the SOE shown in Eq. (12)] is also computed using Eq. (14). In this application example,  $[K^{\epsilon_1}]$  is zero, but since  $[M^{\epsilon_2}]$  is not zero, the real part of the acceleration vector [computed in Eq. (20)] is used as follows:

$$\begin{Bmatrix} A_1^{\epsilon_2} \\ A_2^{\epsilon_2} \end{Bmatrix} = [M^{Re}]^{-1} \left\{ \begin{Bmatrix} F_1^{\epsilon_2} \\ F_2^{\epsilon_2} \end{Bmatrix} - [C^{\epsilon_2}] \begin{Bmatrix} V_1^{Re} \\ V_2^{Re} \end{Bmatrix} - [C^{Re}] \begin{Bmatrix} V_1^{\epsilon_2} \\ V_2^{\epsilon_2} \end{Bmatrix} - [K^{\epsilon_2}] \begin{Bmatrix} U_1^{Re} \\ U_2^{Re} \end{Bmatrix} - [K^{Re}] \begin{Bmatrix} U_1^{\epsilon_2} \\ U_2^{\epsilon_2} \end{Bmatrix} - [M^{\epsilon_2}] \begin{Bmatrix} A_1^{Re} \\ A_2^{Re} \end{Bmatrix} \right\} \quad (22)$$

Finally, the second-order mixed nonreal part of the acceleration vector is computed using the real part [Eq. (20)] and the first-order nonreal parts [Eqs. (21) and (22)] of the acceleration vector, as shown next:

$$\begin{Bmatrix} A_1^{\epsilon_{12}} \\ A_2^{\epsilon_{12}} \end{Bmatrix} = [M^{Re}]^{-1} \left\{ \begin{Bmatrix} F_1^{\epsilon_{12}} \\ F_2^{\epsilon_{12}} \end{Bmatrix} - [C^{\epsilon_{12}}] \begin{Bmatrix} V_1^{Re} \\ V_2^{Re} \end{Bmatrix} - [C^{\epsilon_2}] \begin{Bmatrix} V_1^{\epsilon_1} \\ V_2^{\epsilon_1} \end{Bmatrix} - [C^{\epsilon_1}] \begin{Bmatrix} V_1^{\epsilon_2} \\ V_2^{\epsilon_2} \end{Bmatrix} - [C^{Re}] \begin{Bmatrix} V_1^{\epsilon_{12}} \\ V_2^{\epsilon_{12}} \end{Bmatrix} - [K^{\epsilon_{12}}] \begin{Bmatrix} U_1^{Re} \\ U_2^{Re} \end{Bmatrix} - [K^{\epsilon_2}] \begin{Bmatrix} U_1^{\epsilon_1} \\ U_2^{\epsilon_1} \end{Bmatrix} - [K^{\epsilon_1}] \begin{Bmatrix} U_1^{\epsilon_2} \\ U_2^{\epsilon_2} \end{Bmatrix} - [K^{Re}] \begin{Bmatrix} U_1^{\epsilon_{12}} \\ U_2^{\epsilon_{12}} \end{Bmatrix} - [M^{\epsilon_{12}}] \begin{Bmatrix} A_1^{Re} \\ A_2^{Re} \end{Bmatrix} - [M^{\epsilon_2}] \begin{Bmatrix} A_1^{\epsilon_1} \\ A_2^{\epsilon_1} \end{Bmatrix} - [M^{\epsilon_1}] \begin{Bmatrix} A_1^{\epsilon_2} \\ A_2^{\epsilon_2} \end{Bmatrix} \right\} \quad (23)$$

The matrices in Eqs. (20–23) are included in the Appendix. Moreover, these matrices are filled with real-valued numbers and the only requirement is to invert diagonal matrices, allowing one to use any CDM solver to update the solution vectors ( $\{U^*\}$ ,  $\{V^*\}$ ,  $\{A^*\}$ ,  $\{F^*\}$ ) at each time step.

4) The real and nonreal axes are separated, and the sensitivities are postprocessed. Here, we show the expressions for the nodal displacements but the procedure is the same for the remaining solution vectors:

$$\begin{aligned} \{U\} &= \text{Real}\{\{U^*\}\} = \{U_1^{Re}, U_2\} \\ \frac{\partial \{U\}}{\partial E} &= \text{Im}_{\epsilon_1}\{\{U^*\}\} = \{U_1^{\epsilon_1}, U_2^{\epsilon_1}\} \\ \frac{\partial \{U\}}{\partial \rho} &= \text{Im}_{\epsilon_2}\{\{U^*\}\} = \{U_1^{\epsilon_2}, U_2^{\epsilon_2}\} \\ \frac{\partial^2 \{U^*\}}{\partial E \partial \rho} &= \text{Im}_{\epsilon_{12}}\{\{U^*\}\} = \{U_1^{\epsilon_{12}}, U_2^{\epsilon_{12}}\} \end{aligned} \quad (24)$$

## IV. Verification

To verify the ZSFEM, a one-dimensional truss fixed at both ends and subjected to a sudden axial uniformly distributed load at time  $t = 0$  is studied. Figure 4 displays a schematic of the problem. The parameters for the model are as follows: Young's modulus  $E = 200$  GPa, density  $\rho = 7800$  kg/m<sup>3</sup>, cross-sectional area  $A_{cs} = 5$  mm<sup>2</sup>, length of the truss  $L = 100$  mm, sudden axial distributed load amplitude  $q = 2$  N/mm, and Rayleigh's mass proportional damping parameter  $c_\alpha = 0$ .

The analytical solution for the steady-state displacement response is given by the following expression [95]:

$$U(x, t) = \frac{4qL^2}{\pi^3 EA_{cs}} \sum_{j=1,3,5,\dots}^{\infty} \frac{1}{j^3} \sin\left(\frac{j\pi x}{L}\right) \left(1 - \cos\left(\frac{j\pi ct}{L}\right)\right) \quad (25)$$

A convergence analysis was performed over the first- and second-order analytical sensitivities with respect the Young's modulus. This was done to identify the correct number of terms in the summation necessary to reach stable results. Figure 5 shows the results of this convergence analysis. The results indicate that 1001 terms yield stable results for the real part and the first- and second-order sensitivities. Hereafter, the analytical solution will be calculated using 1001 terms as the reference solution.

### A. Time-Refinement Analysis

A refinement analysis was performed to study the stability of the time discretization used in the CDM. The accuracy between the numerical and the analytical results was analyzed by computing the normalized root-mean-squared deviation [NRMSD; see Eq. (28)]. The analysis includes the real-valued results, the first-order and second-order normalized sensitivities of the displacement with respect to the Young's modulus [see Eqs. (26) and (27) for the nondimensionalization rule].

$$S_y^x = \frac{\partial x}{\partial y} \times |y| \quad (26)$$

$$S_{yz}^x = \frac{\partial^2 x}{\partial y \partial z} \times |yz| \quad (27)$$

$$\text{NRMSD} = \frac{\sqrt{(1/N) \sum_j^N (y_j^{\text{Analytical}} - y_j^{\text{Numerical}})^2}}{\max(y^{\text{Analytical}}) - \min(y^{\text{Analytical}})} \quad (28)$$

Note that 100 spectral truss elements with length  $h_e = 1$  mm, with order of interpolation functions  $p = 19$ , were used to minimize inaccuracies produced by the mesh discretization. The results were obtained at the midpoint of the truss. Figure 6 shows the NRMSD results for the real displacement and its first- and second-order

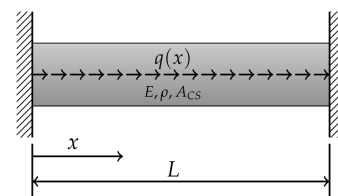
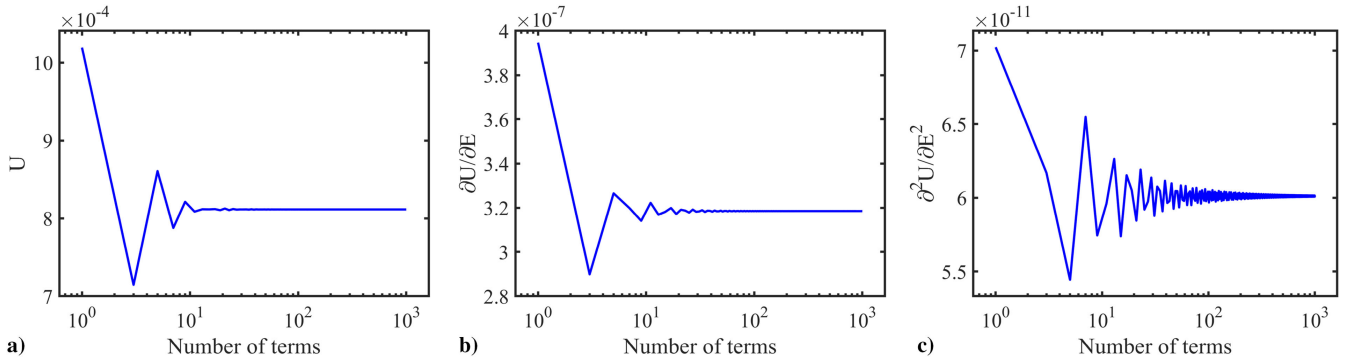
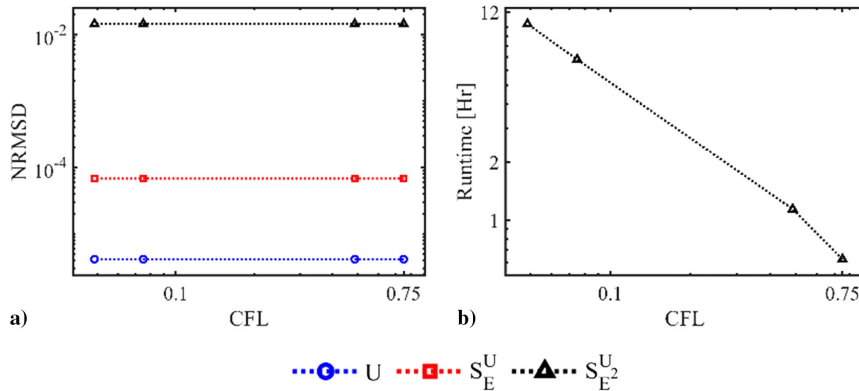


Fig. 4 One-dimensional truss with sudden distributed axial load.



**Fig. 5** a) Convergence analysis of the analytical solution. b) First-order and c) second-order sensitivities with respect to the Young’s modulus at time  $t = 2 \times 10^{-4}$  s and position  $x = L/2$  mm.



**Fig. 6** Time discretization stability analysis: a) accuracy and b) runtime.

sensitivities with respect to the Young’s modulus. These results show that, once the CFL stability condition is met, further reduction in the time step used in the simulations has little influence on the accuracy of the results; for this reason, the CFL was set to 0.75 for subsequent analyses. This value of CFL provides a good balance of accuracy and computational runtime [89].

**B. Mesh Convergence Analysis**

A mesh convergence analysis was performed to study the effect that the size of the spectral elements ( $h$ -refinement) and the order of the interpolation functions used ( $p$ -refinement) have on the accuracy of both the real-value solution and its nondimensional sensitivities. The mesh convergence analysis was performed for elements with varying lengths  $h_e$  between 1 and 50 mm using interpolation functions with varying orders  $p$  from 1 to 19.

Figures 7 and 8 show the results of the mesh convergence analysis. In Fig. 7, we show the accuracy of the results as a function of the inverse of the elements’ size  $1/h_e$  for elements with different order of

interpolation functions  $p$ . Conversely, in Fig. 8, we show the accuracy of the results as a function of the interpolation functions  $p$  for elements with different size  $1/h_e$ . The convergence rate for both  $h$ - and  $p$ -refinements is shown in each figure as a gray triangle (1.682, 1.026, and 0.35 for the  $h$ -refinement and 2.932, 1.964, and 0.802 for the  $p$ -refinement of the displacement and its first- and second-order sensitivities, respectively). The convergence rates indicate that increasing the order of the interpolation functions ( $p$ -refinement) results in a better convergence rate than refining the size of the elements ( $h$ -refinement). This trend holds for first- and second-order sensitivities. However, it is noted that both convergence rates decrease as the order of the sensitivity grows. Previous works using ZFEM have reported a similar result, where, as the order of sensitivity increases, the error also tends to increase. This behavior can be attributed to the fact that higher-order sensitivities depend on lower-order sensitivities and the real part of the solution [56].

From the mesh convergence analysis in Figs. 7 and 8, it is observed that several combinations of mesh size ( $h_e$ ) and order of interpolation

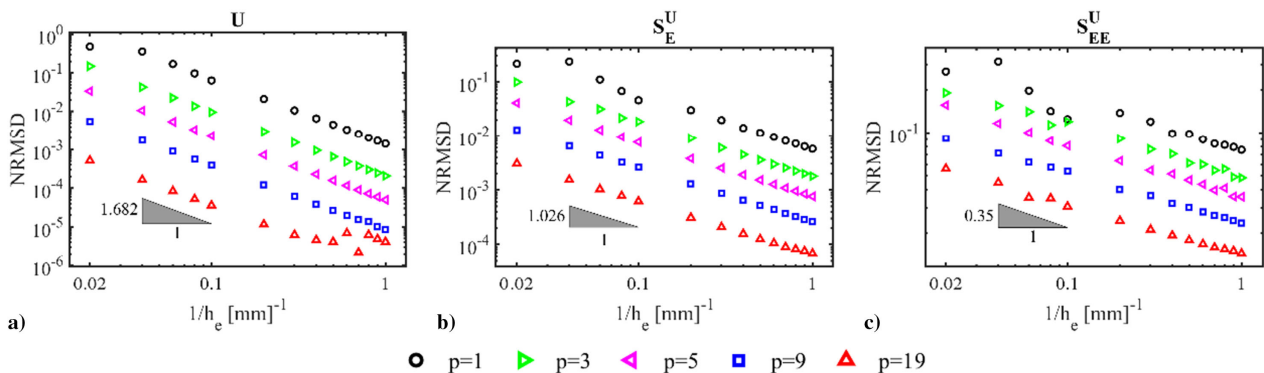


**Fig. 7** The  $h$ -refinement for the real part (a) of the displacement, and the first-order (b) and the second-order (c) sensitivity.

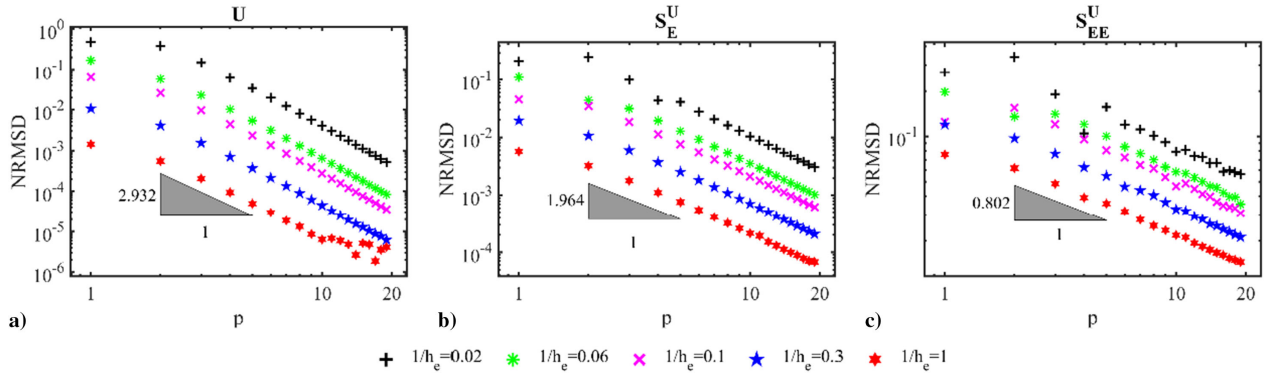


**Fig. 8** The  $p$ -refinement for the real part (a) of the displacement, and the first-order (b) and the second-order (c) sensitivity.

functions ( $p$ ) produce the same accuracy (NRMSD). To investigate this, the isocurves that pass through the point at  $1/h_e = p = 1$  are overlaid in Fig. 9a. The isocurves of the NRMSD values for the displacement and its first- and second-order sensitivities with respect to the Young's modulus are represented with the continuous blue, discontinuous red line, and discontinuous black line, respectively. Figure 9b shows the runtime behavior for these isocurves recovered as reported by ABAQUS in the status file (\*.sta) as "Wallclock time" using one core in an Intel Xeon Gold 6248 CPU at 2.50 GHz and 376 GB of RAM. Figure 9c shows the number of active degrees of freedom. Two additional markers are included in Fig. 9: the magenta triangle represents the behavior when using 100 linear ( $p = 1$ ) elements with length  $h_e = 1$  mm, and the green star represents the behavior when using 2 elements with  $p = 14$  and length  $h_e = 50$  mm. Even though both points yield the same accuracy for the real-valued displacement, we see that both combinations of parameters required similar runtimes with a significant reduction in the number of active degrees of freedom. This trend is preserved for the first- and second-order sensitivity, showing that  $p$ -refinement should be favored over  $h$ -refinement.

### C. Sensitivity Analysis

Analytical and numerical results obtained with ZSFEM are compared for the displacement and its first- and second-order sensitivities evaluated at the center of the truss. The five variables of interest for this sensitivity analysis are the Young's modulus  $E$ , the density  $\rho$ , the cross-sectional area  $A_{cs}$ , the length of the truss  $L$ , and the amplitude of the applied load  $q$ . For the numerical results, we used 100 spectral truss elements with length  $h_e = 1$  mm and interpolation functions of order  $p = 19$ , corresponding to the most refined values evaluated in the mesh convergence analysis. These results are compared against the analytical solution in Eq. (25) and the sensitivities obtained from the analytical solution using the symbolic algebra package from

MATLAB. The NRMSD [see Eq. (28)] was used as a measure of error. Figure 10 shows the results for the displacement and its first-order sensitivities. Excellent agreement was found for the displacement with an NRMSD value of  $4 \times 10^{-6}$  and the first-order sensitivities with a maximum NRMSD value of  $4 \times 10^{-3}$ .

Second-order sensitivities and mixed sensitivities we are also verified (see Fig. 11). The analysis includes sensitivities of the displacement at the center of the truss with respect to a mechanical parameter (the Young's modulus), a geometric parameter (the length of the truss), and a boundary condition (the amplitude of the applied load). The excellent agreement is preserved with maximum NRMSD values of  $10^{-2}$  for second-order sensitivities.

### D. Comparison with the Finite Differences Method

The finite differences method (FDM) is the most traditional method to obtain numerical sensitivities due to its simplicity. For this reason, in this section we compare the performance and accuracy of ZSFEM and FDM. For this comparison, a central difference scheme with second-order accuracy was used, as detailed in Eqs. (29) and (30) for the first- and second-order sensitivities of the displacement with respect an input parameter  $\alpha$ , where the term  $h$  is the magnitude of the perturbation step.

$$\frac{\partial U(\alpha)}{\partial \alpha} = \frac{U(\alpha + h) - U(\alpha - h)}{2h} + O(h^2) \quad (29)$$

$$\frac{\partial^2 U(\alpha)}{\partial \alpha^2} = \frac{U(\alpha + h) - 2U(\alpha) + U(\alpha - h)}{h^2} + O(h^2) \quad (30)$$

Table 1 presents the runtimes for both methods, which have been normalized by the runtime of a single real-valued simulation. The computational overhead observed in our method can be attributed to the following factors:

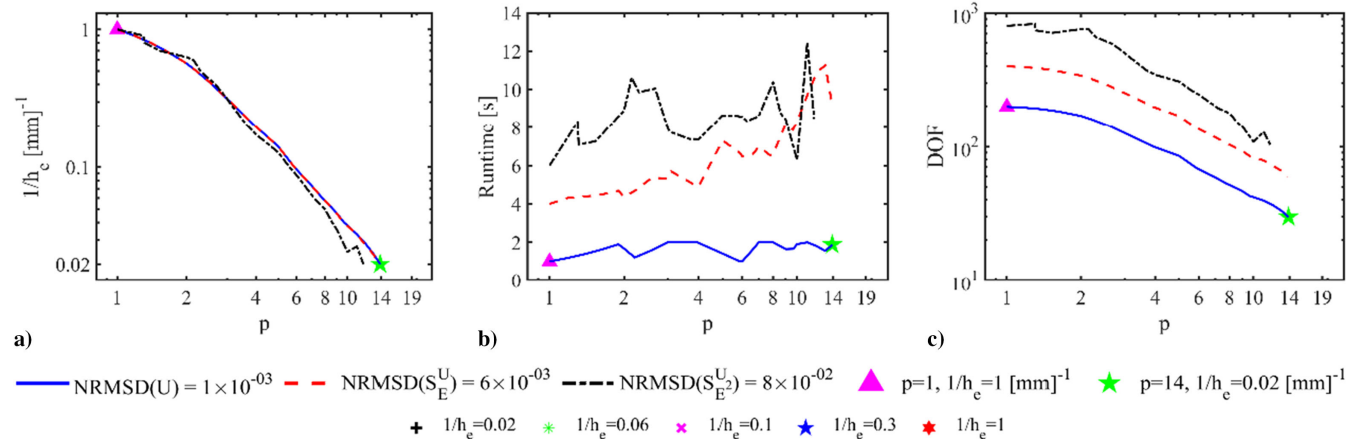


**Fig. 9** Isocurves of NRMSD through  $1/h_e = p = 1$  as function of  $p$ . a) Equivalent inverse of elements' size  $1/h_e$ , b) computational runtime, and c) number of active degrees of freedom.

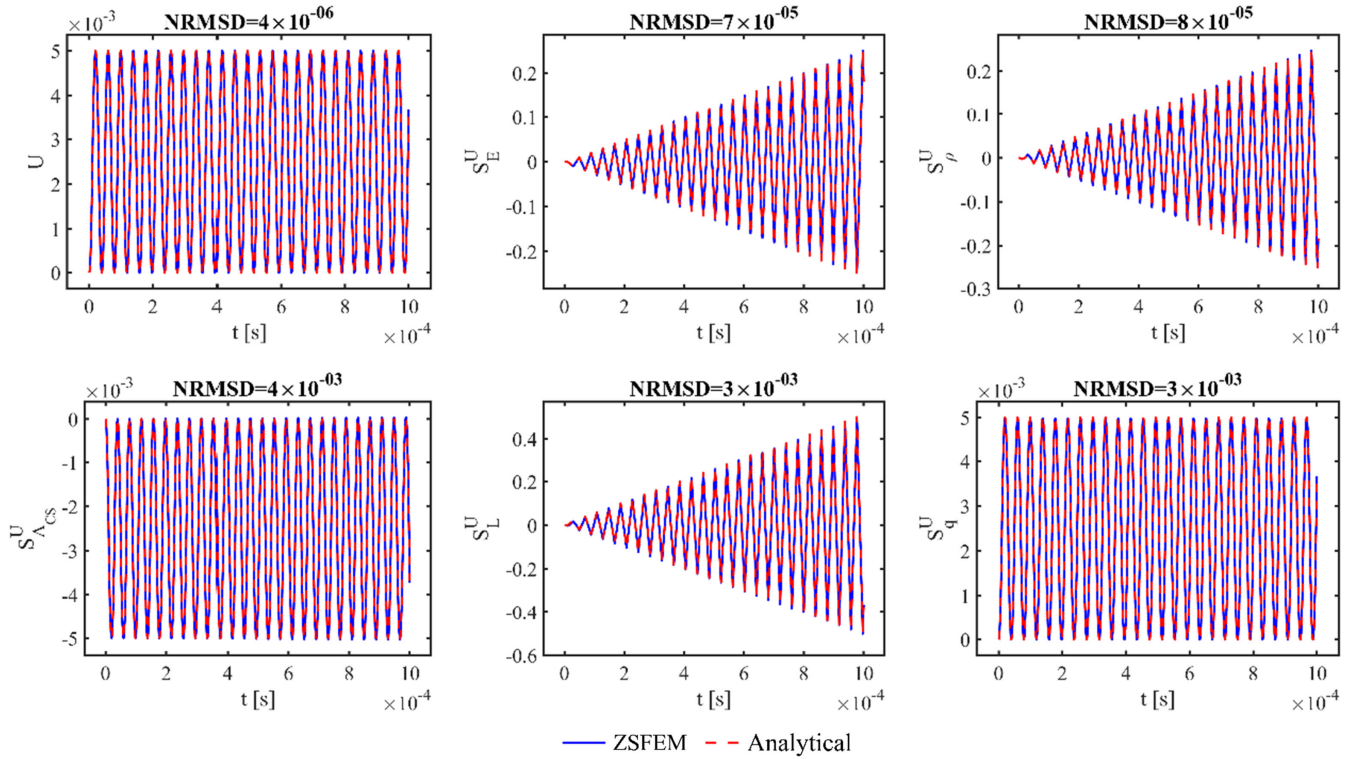


Fig. 10 Comparison of numerical and analytical results for the displacement at the center of the truss and first-order sensitivities.

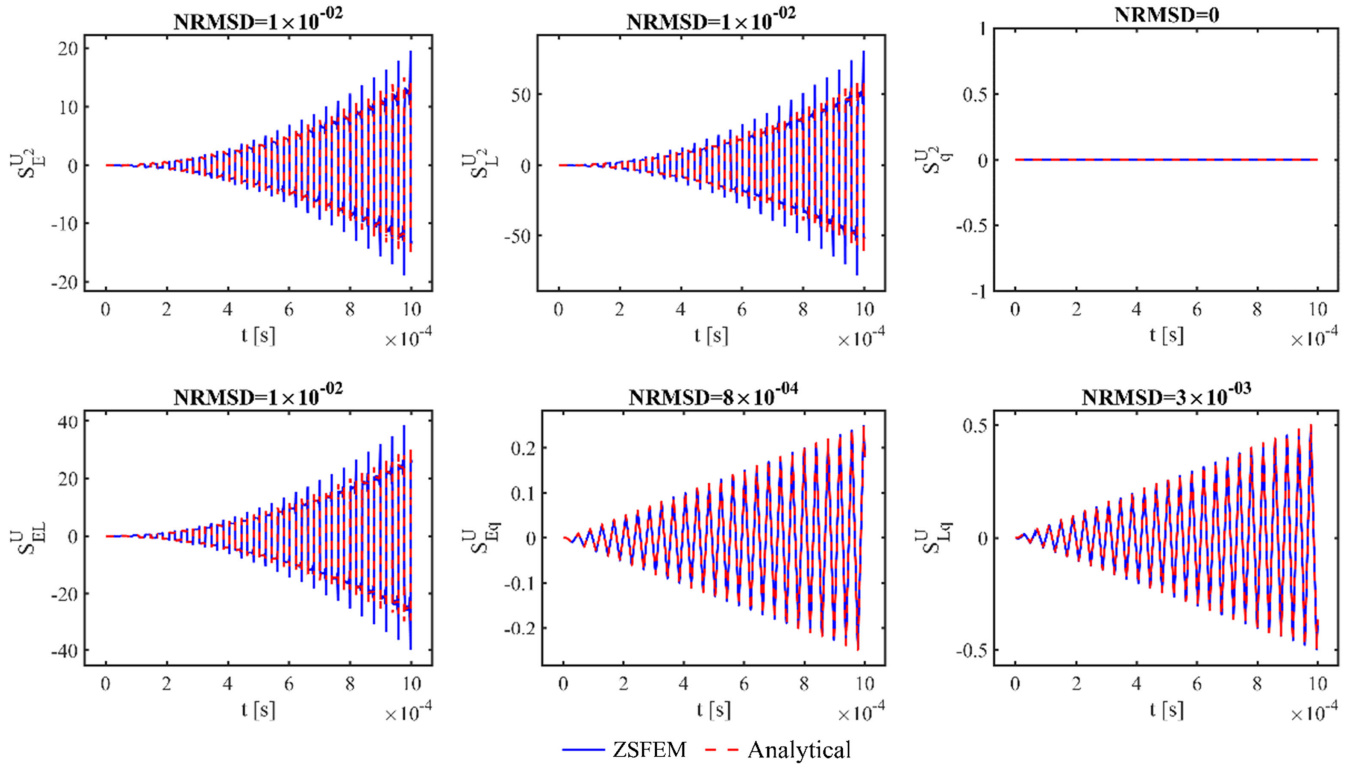


Fig. 11 Comparison of numerical and analytical second-order sensitivities of the displacement.

i) ZSFEM allows for the simultaneous computation of higher-order sensitivities, including all lower-order sensitivities, in a single run. In contrast, FDM requires multiple reruns of the simulation to compute a single sensitivity at a specific order. This fundamental difference in approach leads to a higher computational cost for FDM.

ii) To compute sensitivities with ZSFEM, we rely on external libraries that handle algebraic operations using hyper-dual numbers.

This is necessary because traditional programming languages do not natively support this type of algebra. As a result, operator overloading is required, which can lead to a reduction in performance compared to specialized implementations. However, this tradeoff enables the accurate computation of sensitivities with ZSFEM.

Furthermore, it is worth highlighting that FDM is highly sensitive to the selection of the perturbation step size  $h$  due to truncation and

**Table 1 Runtime comparison required by FDM and ZSFEM to compute first- and second-order sensitivities**

Method	$S_E^U$	$S_{E^2}^U$
ZSFEM	$\times 1.46$	$\times 1.74$
FDM	$\times 2.00$	$\times 3.00$

subtraction round-off errors. Finding the ideal perturbation step that maximizes the accuracy of FDM requires multiple iterations, adding significant computational overhead. Also, the ideal perturbation step is problem-dependent and cannot be generalized, making it challenging to determine in practice. The runtimes reported in Table 1 assume that the ideal perturbation step is known and only a single iteration is necessary for FDM, which in most cases is far from reality.

A convergence analysis over the perturbation step size  $h$  was performed to compare the accuracy of FDM and ZSFEM. The accuracy was measured using the NRMSD between numerical and analytical results. Figure 12 shows the error convergence for the displacement and its first- and second-order sensitivities with respect to the Young's modulus. Note that the accuracy obtained with FDM varies several orders of magnitude as a function of the perturbation step magnitude used, reaching a minimum value when both truncation and cancellation errors are minimized,  $h = 10^{-3}$  for first-order and  $h = 10^{-4}$  for second order. In contrast, the accuracy of ZSFEM is shown to be independent of the perturbation step magnitude and always superior to the best accuracy reached with FDM. It is also important to remark here that as the higher-order sensitivities are

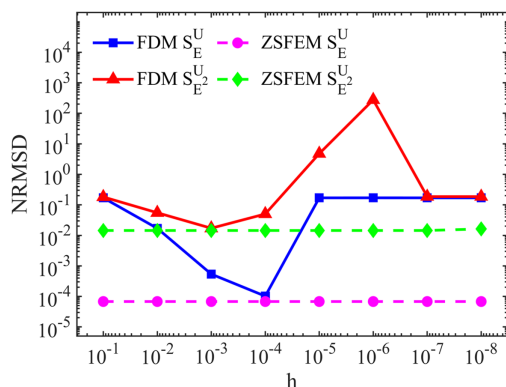


**Fig. 12 Comparison of normalized root-mean-squared deviation for first- and second-order sensitivities obtained with ZSFEM and FDM.**

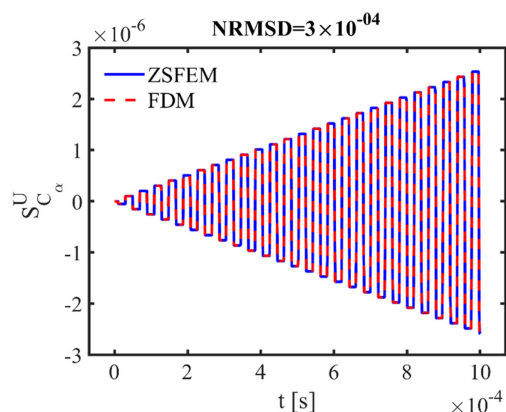


**Fig. 13 Comparison of sensitivity of the displacement with respect to the Rayleigh's damping parameter  $C_\alpha$ .**

computed using the results of the lower-order sensitivities, the error propagates, and therefore the error increases with the order of the sensitivities

Although the analytical solution in Eq. (25) does not consider the contribution of damping, we highlight that with ZSFEM it is possible to obtain the sensitivities of the displacement with respect each of the Rayleigh's damping parameters. The first-order sensitivity of the displacement with respect to  $C_\alpha$  was computed using ZSFEM and FDM [see Eq. (29)]. The comparison of both results is shown in Fig. 13 using  $C_\alpha = C_\beta = 10^{-10}$ . Excellent agreement between both results was obtained with an NRMSD value of  $3 \times 10^{-4}$ .

## V. Conclusions

In this paper, the hypercomplex Taylor series expansion (ZTSE) differentiation theory is coupled with the time-domain spectral finite elements method (SFEM), yielding the hypercomplex spectral finite elements method (ZSFEM). This methodology enables the calculation of highly accurate arbitrary-order sensitivities with respect to mechanical parameters, geometry, and boundary conditions in mechanical wave propagation problems. Although ZSFEM takes advantage of hypercomplex algebra to obtain sensitivities, the method does not require hypercomplex-variable solvers. Instead, the equation of motion is solved using the CR notation of hypercomplex numbers, and operations involving hypercomplex variables are carried out with external libraries. This transformation allows to implement ZSFEM in any real-valued solver facilitating the implementation of the new method within commercial finite element software (e.g., Abaqus).

A test case with a known analytical solution was used to quantify the accuracy of ZSFEM. Excellent agreement was found between analytical and numerical sensitivities with a maximum NRMSD of  $10^{-2}$ . Also, mesh-convergence analyses were performed as a function of the order of the interpolation functions  $p$  ( $p$ -refinement) and the size  $h_e$  of the elements ( $h$ -refinement), revealing that  $p$ -refinement offers better convergence rates than  $h$ -refinement. This trend was consistent in the real-valued analysis and in the computation of first- and second-order sensitivities. Subsequently, ZSFEM was compared against the FDM, revealing that ZSFEM is capable of achieving better accuracy than FDM in less computational runtime. Moreover, the accuracy of ZSFEM was proven to be insensitive to the selection of perturbation step size. This feature removes the need of iterating to find the accurate step size to minimize computing errors, which is a characteristic feature of FDM. Although we believe that the same trend will hold in problems incorporating other types of elements (e.g., 2D plane elements, 3D brick elements, Shell elements), further investigation is required.

We demonstrated that using hypercomplex algebra for sensitivity analysis in wave propagation problems did not require modifications to the formulation of existing SFEM elements. The framework presented in this work can be applied to other element formulations and discretization methods, such as the boundary elements method and the more recent C1-continuous time-domain SFEM [96–98]. These implementations will be considered in future research.

Although the development of ZSFEM was presented using Truss elements, ZSFEM is general and can be applied to continuum and shell elements. This characteristic feature is of high importance as it increases the impact of the proposed methodology and enables its implementation in problems of different fields, such as mechanical wave propagation, SHM, nondestructive evaluation, acoustics, structural dynamics, strain-dependent analysis, high-velocity impact, drop testing, seismic analysis, metal rolling, and energy dissipation. Furthermore, access to highly accurate sensitivities of arbitrary-order provided by ZSFEM is advantageous because it enables a better understanding of the effect that deviations from modeled design conditions can have on the dynamic behavior of a structure. And it also promotes new developments in sensitivity analysis, uncertainty quantification, optimization, error analysis, stability analysis, and computational model-assisted decision making. We posit that ZSFEM will constitute a fundamental development in a wide number

of fields that require modeling of transient dynamic phenomena while simultaneously providing highly accurate sensitivity information.

**Appendix A: Cauchy–Riemann Notation**

Hypercomplex variables and their operations are not supported in most numerical packages. However, it is possible to take advantage of the hypercomplex algebra isomorphism to represent both multicomplex and hyper-dual numbers as a matrix completely filled with real numbers. This representation of hypercomplex numbers is known as the Cauchy–Riemann (CR) matrix form and replaces the operations between hypercomplex numbers [80] with matrix functions and arithmetic operations. For example, hyper-dual numbers of order  $\eta$  are defined as the addition of two hyper-dual numbers of order  $\eta - 1$ ,  $\mathbb{D}^\eta = \{z^*/z^* = a_1^* + a_2^*e_\eta; a_1^*, a_2^* \in \mathbb{D}^{\eta-1}\}$ , and considering that  $\mathbb{D}^0 \equiv \mathbb{R}$ , the CR matrix form of  $z^*$  follows the next recursive rule:

$$[z^*] = \begin{bmatrix} [a_1^*] & 0 \\ [a_1^*] & [a_1^*] \end{bmatrix}; [z^*] \in \mathbb{R}^{2^\eta \times 2^\eta}; [a_1^*], [a_2^*] \in \mathbb{R}^{2^{\eta-1} \times 2^{\eta-1}} \quad (A1)$$

In the case of dual numbers,  $\mathbb{D}^1 = \{z^*/z^* = a_1^* + a_2^*e_1; a_1^*, a_2^* \in \mathbb{D}^0\}$ . Thus, the CR matrix form is

$$[z^*] = \begin{bmatrix} a_1 & 0 \\ a_2 & a_1 \end{bmatrix}; [z^*] \in \mathbb{R}^{2 \times 2}; a_1, a_2 \in \mathbb{R} \quad (A2)$$

This time, a bi-dual number is considered,  $\mathbb{D}^2 = \{z^*/z^* = a_1^* + a_2^*e_2; a_1^*, a_2^* \in \mathbb{D}^1\}$ , where  $a_1^* = b_1 + b_2e_1$  and  $a_2^* = b_3 + b_4e_1$ . Thereafter,  $z^* = b_1 + b_2e_1 + b_3e_2 + b_4e_{12}$ , and the corresponding CR representation is

$$[z^*] = \begin{bmatrix} [a_1^*] & 0 \\ [a_2^*] & [a_1^*] \end{bmatrix} = \begin{bmatrix} b_1 & 0 & 0 & 0 \\ b_2 & b_1 & 0 & 0 \\ b_3 & 0 & b_1 & 0 \\ b_4 & b_3 & b_2 & b_1 \end{bmatrix}; [z^*] \in \mathbb{R}^{4 \times 4}; b_1, b_2, b_3, b_4 \in \mathbb{R} \quad (A3)$$

**Appendix B: Matrices of Step-by-Step Application Example**

The matrices of the step-by-step application example are defined next:

$$[M^*] \approx \frac{A_{cs}(\rho^{Re} + \epsilon_2)(\chi_2 - \chi_1)}{2} \begin{bmatrix} 1 & 0 \\ 0 & 1 \end{bmatrix}$$

$$[K^*] \approx \frac{A_{cs}(E^{Re} + \epsilon_1)}{\chi_2 - \chi_1} \begin{bmatrix} 1 & -1 \\ -1 & 1 \end{bmatrix}$$

$$[C^*] \approx \frac{A_{cs}c_a^{Re} \rho^{Re}(\chi_2 - \chi_1)}{2} \begin{bmatrix} 1 & 0 \\ 0 & 1 \end{bmatrix} + \frac{A_{cs}E^{Re} C_\beta^{Re}}{\chi_2 - \chi_1} \begin{bmatrix} 1 & -1 \\ -1 & 1 \end{bmatrix} \quad (B1)$$

The real components correspond to

$$[M^{Re}] \approx \frac{A_{cs}\rho^{Re}(\chi_2 - \chi_1)}{2} \begin{bmatrix} 1 & 0 \\ 0 & 1 \end{bmatrix}$$

$$[K^{Re}] \approx \frac{A_{cs}E^{Re}}{\chi_2 - \chi_1} \begin{bmatrix} 1 & -1 \\ -1 & 1 \end{bmatrix}$$

$$[C^{Re}] \approx \frac{A_{cs}c_a^{Re} \rho^{Re}(\chi_2 - \chi_1)}{2} \begin{bmatrix} 1 & 0 \\ 0 & 1 \end{bmatrix} + \frac{A_{cs}E^{Re} C_\beta^{Re}}{\chi_2 - \chi_1} \begin{bmatrix} 1 & -1 \\ -1 & 1 \end{bmatrix} \quad (B2)$$

The nonreal components correspond to

$$[M^{\epsilon_1}] \approx \begin{bmatrix} 0 & 0 \\ 0 & 0 \end{bmatrix}$$

$$[M^{\epsilon_2}] \approx \frac{A_{cs}(\chi_2 - \chi_1)}{2} \begin{bmatrix} 1 & 0 \\ 0 & 1 \end{bmatrix}$$

$$[K^{\epsilon_2}] \approx \begin{bmatrix} 0 & 0 \\ 0 & 0 \end{bmatrix}$$

$$[C^{\epsilon_2}] \approx \begin{bmatrix} 0 & 0 \\ 0 & 0 \end{bmatrix}$$

$$[M^{\epsilon_{12}}] \approx \begin{bmatrix} 0 & 0 \\ 0 & 0 \end{bmatrix}$$

$$[K^{\epsilon_{12}}] \approx \begin{bmatrix} 0 & 0 \\ 0 & 0 \end{bmatrix}$$

$$[C^{\epsilon_{12}}] \approx \begin{bmatrix} 0 & 0 \\ 0 & 0 \end{bmatrix} \quad (B3)$$

**Acknowledgments**

The authors would like to acknowledge the support from the Office of Naval Research program managers Anisur Rahman and Bill Nickerson (grant number N00014-21-1-2428) and the United States Army Research Office (grants number W911NF2010315 and W911NF2310192). Juan D. Navarro also would like to acknowledge the support of the Roberto Rocca Educational Program.

**References**

- [1] Sinou, J. J., “A Review of Damage Detection and Health Monitoring of Mechanical Systems from Changes in the Measurement of Linear and Non-Linear Vibrations,” *Mechanical Vibrations: Measurement, Effects and Control*, Nova Science Publ., Inc., Hauppauge, NY, 2009, pp. 643–702.
- [2] Willberg, C., Duczek, S., Vivar-Perez, J. M., and Ahmad, Z. A. B., “Simulation Methods for Guided Wave-Based Structural Health Monitoring: A Review,” *Applied Mechanics Reviews*, Vol. 67, No. 1, 2015, pp. 1–20. <https://doi.org/10.1115/1.4029539>
- [3] Su, Z., Ye, L., and Lu, Y., “Guided Lamb Waves for Identification of Damage in Composite Structures: A Review,” *Journal of Sound and Vibration*, Vol. 295, Nos. 3–5, 2006, pp. 753–780. <https://doi.org/10.1016/j.jsv.2006.01.020>
- [4] Deraemaeker, A., *New Trends in Vibration Based Structural Health Monitoring*, Springer, Berlin, 2010, pp. 1–38.
- [5] Palacz, M., “Spectral Methods for Modelling of Wave Propagation in Structures in Terms of Damage Detection—A Review,” *Applied Sciences*, Vol. 8, No. 7, 2018, p. 1124. <https://doi.org/10.3390/app8071124>
- [6] Ostachowicz, W., Soman, R., and Malinowski, P., “Optimization of Sensor Placement for Structural Health Monitoring: A Review,” *Structural Health Monitoring*, Vol. 18, No. 3, 2019, pp. 963–988. <https://doi.org/10.1177/1475921719825601>
- [7] Soman, R., Kudela, P., Balasubramaniam, K., Singh, S. K., and Malinowski, P., “A Study of Sensor Placement Optimization Problem for Guided Wave-Based Damage Detection,” *Sensors (Switzerland)*, Vol. 19, No. 8, 2019, p. 1856. <https://doi.org/10.3390/s19081856>
- [8] Capellari, G., Chatzi, E., and Mariani, S., “Cost–Benefit Optimization of Structural Health Monitoring Sensor Networks,” *Sensors*, Vol. 18, No. 7, 2018, p. 2174. <https://doi.org/10.3390/s18072174>
- [9] Lee, B. C., and Staszewski, W. J., “Sensor Location Studies for Damage Detection with Lamb Waves,” *Smart Materials and Structures*, Vol. 16, No. 2, 2007, pp. 399–408. <https://doi.org/10.1088/0964-1726/16/2/019>
- [10] Mallardo, V., and Aliabadi, M. H., “Optimal Sensor Placement for Structural, Damage and Impact Identification: A Review,” *Structural Durability & Health Monitoring*, Vol. 9, No. 4, 2013, pp. 287–323. <https://doi.org/10.32604/sdhm.2013.009.287>

- [11] Capellari, G., Chatzi, E., and Mariani, S., “Cost-Benefit Optimization of Sensor Networks for SHM Applications,” No. 2, 2017, p. 132.
- [12] Swillam, M. A., Bakr, M. H., and Li, X., “Full Wave Sensitivity Analysis of Guided Wave Structures Using FDTD,” *Journal of Electromagnetic Waves and Applications*, Vol. 22, No. 16, 2008, pp. 2135–2145. <https://doi.org/10.1163/156939308787522474>
- [13] Xie, Z., Komatitsch, D., Martin, R., and Matzen, R., “Improved Forward Wave Propagation and Adjoint-Based Sensitivity Kernel Calculations Using a Numerically Stable Finite-Element PML,” *Geophysical Journal International*, Vol. 198, No. 3, 2014, pp. 1714–1747. <https://doi.org/10.1093/gji/ggu219>
- [14] Martins, J. R. R. A., and Hwang, J. T., “Review and Unification of Methods for Computing Derivatives of Multidisciplinary Computational Models,” *AIAA Journal*, Vol. 51, No. 11, 2013, pp. 2582–2599. <https://doi.org/10.2514/1.J052184>
- [15] Konstantinidis, G., Drinkwater, B. W., and Wilcox, P. D., “The Temperature Stability of Guided Wave Structural Health Monitoring Systems,” *Smart Materials and Structures*, Vol. 15, No. 4, 2006, pp. 967–976. <https://doi.org/10.1088/0964-1726/15/4/010>
- [16] Lee, B. C., Manson, G., and Staszewski, W. J., “Environmental Effects on Lamb Wave Responses from Piezoceramic Sensors,” *Materials Science Forum*, Vols. 440–441, Trans Tech Publ., Switzerland, 2003, pp. 195–202. <https://doi.org/10.4028/www.scientific.net/MSF.440-441.195>
- [17] Sohn, H., “Effects of Environmental and Operational Variability on Structural Health Monitoring,” *Philosophical Transactions of the Royal Society A: Mathematical, Physical and Engineering Sciences*, Vol. 365, No. 1851, 2007, pp. 539–560. <https://doi.org/10.1098/rsta.2006.1935>
- [18] Mitra, M., and Gopalakrishnan, S., “Guided Wave Based Structural Health Monitoring: A Review,” *Smart Materials and Structures*, Vol. 25, No. 5, 2016, Paper 053001. <https://doi.org/10.1088/0964-1726/25/5/053001>
- [19] Sridaran Venkat, R., Boller, C., Ravi, N. B., Chakraborty, N., Kamalakar, G. S., Ukirde, K., and Mahapatra, D. R., “Optimized Actuator/Sensor Combinations for Structural Health Monitoring: Simulation and Experimental Validation,” *Structural Health Monitoring 2015: System Reliability for Verification and Implementation—Proceedings of the 10th International Workshop on Structural Health Monitoring, IWSHM 2015*, Vol. 2, DEStech Publ., Inc., Lancaster, PA, 2015, pp. 1014–1021. <https://doi.org/10.12783/shm2015/128>
- [20] Ewald, V., Groves, R., and Benedictus, R., “Transducer Placement Option of Lamb Wave SHM System for Hotspot Damage Monitoring,” *Aerospace*, Vol. 5, No. 2, 2018, p. 39. <https://doi.org/10.3390/aerospace5020039>
- [21] Iott, J., Hafika, R. T., and Adelman, H. M., “Selecting Step Sizes in Sensitivity Analysis By Finite Differences,” NASA TM-86382, Aug. 1985.
- [22] Mathur, R., “An Analytical Approach to Computing Step Sizes for Finite-Difference Derivatives,” Doctoral Dissertation, Univ. of Texas, Austin, TX, 2012.
- [23] Garza, J., and Millwater, H. R., “Multicomplex Newmark-Beta Time Integration Method for Sensitivity Analysis in Structural Dynamics,” *AIAA Journal*, Vol. 53, No. 5, 2015, pp. 1188–1198. <https://doi.org/10.2514/1.J053282>
- [24] De Pauw, D. J. W., and Vanrolleghem, P. A., “Practical Aspects of Sensitivity Function Approximation for Dynamic Models,” *Mathematical and Computer Modelling of Dynamical Systems*, Vol. 12, No. 5, 2006, pp. 395–414. <https://doi.org/10.1080/13873950600723301>
- [25] Choi, K. K., and Kim, N.-H., *Structural Sensitivity Analysis and Optimization I*, Springer, New York, 2005, pp. 209–414.
- [26] Bischof, C., Khademi, P., Mauer, A., and Carle, A., “Adifor 2.0: Automatic Differentiation of Fortran 77 Programs,” *IEEE Computational Science and Engineering*, Vol. 3, No. 3, 1996, pp. 18–32. <https://doi.org/10.1109/99.537089>
- [27] Voßbeck, M., Giering, R., and Kaminski, T., “Development and First Applications of TAC++,” Lecture Notes in Computational Science and Engineering, Springer, Berlin, 2008, pp. 187–197.
- [28] Hascoet, L., and Pascual, V., “The Tapenade Automatic Differentiation Tool,” *ACM Transactions on Mathematical Software*, Vol. 39, No. 3, 2013, pp. 1–43. <https://doi.org/10.1145/2450153.2450158>
- [29] Margossian, C. C., “A Review of Automatic Differentiation and Its Efficient Implementation,” *WIREs Data Mining and Knowledge Discovery*, Vol. 9, No. 4, 2019, pp. 1–19. <https://doi.org/10.1002/widm.1305>
- [30] Squire, W., and Trapp, G., “Using Complex Variables to Estimate Derivatives of Real Functions,” *SIAM Review*, Vol. 40, No. 1, 1998, pp. 110–112. <https://doi.org/10.1137/S003614459631241X>
- [31] Martins, J. R. R. A., Sturdza, P., and Alonso, J. J., “The Complex-Step Derivative Approximation,” *ACM Transactions on Mathematical Software*, Vol. 29, No. 3, 2003, pp. 245–262. <https://doi.org/10.1145/838250.838251>
- [32] Lantoine, G., Russell, R. P., and Dargent, T., “Using Multicomplex Variables for Automatic Computation of High-Order Derivatives,” *ACM Transactions on Mathematical Software*, Vol. 38, No. 3, 2012, pp. 1–21. <https://doi.org/10.1145/2168773.2168774>
- [33] Fike, J., and Alonso, J., “The Development of Hyper-Dual Numbers for Exact Second-Derivative Calculations,” *49th AIAA Aerospace Sciences Meeting Including the New Horizons Forum and Aerospace Exposition*, AIAA Paper 2011-0886, 2011.
- [34] Clifford, M. A., “Preliminary Sketch of Biquaternions,” *Proceedings of the London Mathematical Society*, Vols. s1-4, No. 1, 1871, pp. 381–395. <https://doi.org/10.1112/plms/s1-4.1.381>
- [35] Spall, R. E., and Yu, W., “Imbedded Dual-Number Automatic Differentiation for Computational Fluid Dynamics Sensitivity Analysis,” *Journal of Fluids Engineering*, Vol. 135, No. 1, 2013, pp. 1–4. <https://doi.org/10.1115/1.4023074>
- [36] Yu, W., and Blair, M., “DNAD, A Simple Tool for Automatic Differentiation of Fortran Codes Using Dual Numbers,” *Computer Physics Communications*, Vol. 184, No. 5, 2013, pp. 1446–1452. <https://doi.org/10.1016/j.cpc.2012.12.025>
- [37] Lin, B., Gresil, M., Cuc, A., and Giurgiutiu, V., “Predictive Modeling of Piezoelectric Wafer Active Sensors for Structural Health Monitoring,” *Ferroelectrics*, Vol. 470, No. 1, 2014, pp. 168–182. <https://doi.org/10.1080/00150193.2014.923251>
- [38] Raghavan, A., and Cesnik, C. E. S., “Finite-Dimensional Piezoelectric Transducer Modeling for Guided Wave Based Structural Health Monitoring,” *Smart Materials and Structures*, Vol. 14, No. 6, 2005, pp. 1448–1461. <https://doi.org/10.1088/0964-1726/14/6/037>
- [39] Peake, M. J., Trevelyan, J., and Coates, G., “Extended Isogeometric Boundary Element Method (XIBEM) for Three-Dimensional Medium-Wave Acoustic Scattering Problems,” *Computer Methods in Applied Mechanics and Engineering*, Vol. 284, Feb. 2015, pp. 762–780. <https://doi.org/10.1016/j.cma.2014.10.039>
- [40] Jin, W., “Semi-Analytical Complex Variable Based Stochastic Finite Element Method,” Doctoral Dissertation, Univ. of Texas, Arlington, TX, 2008.
- [41] Jin, W., Dennis, B. H., and Wang, B. P., “Improved Sensitivity Analysis Using a Complex Variable Semi-Analytical Method,” *Structural and Multidisciplinary Optimization*, Vol. 41, No. 3, 2010, pp. 433–439. <https://doi.org/10.1007/s00158-009-0427-8>
- [42] Martins, J. R. R. A., Kroo, I., and Alonso, J., “An Automated Method for Sensitivity Analysis Using Complex Variables,” *38th Aerospace Sciences Meeting and Exhibit*, AIAA Paper 2000-0689, 2000.
- [43] Vatsa, V., “Computation of Sensitivity Derivatives of Navier–Stokes Equations Using Complex Variables,” *Advances in Engineering Software*, Vol. 31, Nos. 8–9, 2000, pp. 655–659. [https://doi.org/10.1016/S0965-9978\(00\)00025-9](https://doi.org/10.1016/S0965-9978(00)00025-9)
- [44] Anderson, W., Newman, J., Whitfield, D., and Nielsen, E., “Sensitivity Analysis for the Navier-Stokes Equations on Unstructured Meshes Using Complex Variables,” *AIAA Journal*, Vol. 39, No. 1, 1999, pp. 56–63.
- [45] Burg, C. O. E., and Newman, J. C., III, “Computationally Efficient, Numerically Exact Design Space Derivatives via the Complex Taylor’s Series Expansion Method,” *Computers & Fluids*, Vol. 32, No. 3, 2003, pp. 373–383. [https://doi.org/10.1016/S0045-7930\(01\)00044-5](https://doi.org/10.1016/S0045-7930(01)00044-5)
- [46] Cerviño, L. I., and Bewley, T. R., “On the Extension of the Complex-Step Derivative Technique to Pseudospectral Algorithms,” *Journal of Computational Physics*, Vol. 187, No. 2, 2003, pp. 544–549. [https://doi.org/10.1016/S0021-9991\(03\)00123-2](https://doi.org/10.1016/S0021-9991(03)00123-2)
- [47] Newman, J. C., Whitfield, D. L., and Anderson, W. K., “Step-Size Independent Approach for Multidisciplinary Sensitivity Analysis,” *Journal of Aircraft*, Vol. 40, No. 3, 2003, pp. 566–573. <https://doi.org/10.2514/2.3131>
- [48] Kim, J., Bates, D. G., and Postlethwaite, I., “Nonlinear Robust Performance Analysis Using Complex-Step Gradient Approximation,” *Automatica*, Vol. 42, No. 1, 2006, pp. 177–182. <https://doi.org/10.1016/j.automatica.2005.09.008>
- [49] Kim, J., Bates, D. G., and Postlethwaite, I., “Nonlinear Robust Performance Analysis Using Complex-Step Gradient Approximation,” *Automatica*, Vol. 42, No. 1, 2006, pp. 177–182. <https://doi.org/10.1016/j.automatica.2005.09.008>

- [50] Mundstock, D. C., and Marczak, R. J., "Boundary Element Sensitivity Evaluation for Elasticity Problems Using Complex Variable Method," *Structural and Multidisciplinary Optimization*, Vol. 38, No. 4, 2009, pp. 423–428.  
<https://doi.org/10.1007/s00158-008-0283-y>
- [51] Garza, J. E., and Millwater, H. R., "Sensitivity Analysis in Structural Dynamics Using the ZFEM Complex Variable Finite Element Method," *54th AIAA/ASME/ASCE/AHS/ASC Structures, Structural Dynamics, and Materials Conference*, AIAA Paper 2013-1580, 2013.
- [52] Wang, B. P., and Apte, A. P., "Complex Variable Method for Eigen-solution Sensitivity Analysis," *AIAA Journal*, Vol. 44, No. 12, 2006, pp. 2958–2961.  
<https://doi.org/10.2514/1.19225>
- [53] Kim, H., and Cho, M., "Study on the Design Sensitivity Analysis Based on Complex Variable in Eigenvalue Problem," *Finite Elements in Analysis and Design*, Vol. 45, No. 12, 2009, pp. 892–900.  
<https://doi.org/10.1016/j.finel.2009.07.002>
- [54] Fujikawa, M., Tanaka, M., Mitsume, N., and Imoto, Y., "Hyper-Dual Number-Based Numerical Differentiation of Eigensystems," *Computer Methods in Applied Mechanics and Engineering*, Vol. 390, Feb. 2022, Paper 114452.  
<https://doi.org/10.1016/j.cma.2021.114452>
- [55] Velasquez-gonzalez, J. C., Navarro, J. D., Aristizabal, M., Montoya, A., Millwater, H. R., and Restrepo, D., "Arbitrary-Order Sensitivity Analysis of Eigenfrequency Problems Using the Hypercomplex Taylor Series Expansion (ZTSE) Method," *Applied Sciences*, Vol. 13, No. 12, 2023, p. 7125.
- [56] Navarro, J. D., Millwater, H. R., Montoya, A. H., and Restrepo, D., "Arbitrary-Order Sensitivity Analysis in Phononic Metamaterials Using the Multicomplex Taylor Series Expansion Method Coupled with Bloch's Theorem," *Journal of Applied Mechanics*, Vol. 89, No. 2, 2021, pp. 1–43.  
<https://doi.org/10.1115/1.4052830>
- [57] Haveroth, G. A., Stahlschmidt, J., and Muñoz-Rojas, P. A., "Application of the Complex Variable Semi-Analytical Method for Improved Displacement Sensitivity Evaluation in Geometrically Nonlinear Truss Problems," *Latin American Journal of Solids and Structures*, Vol. 12, No. 5, 2015, pp. 980–1005.  
<https://doi.org/10.1590/1679-78251911>
- [58] Jin, W., Dennis, B. H., and Wang, B. P., "Improved Sensitivity and Reliability Analysis of Nonlinear Euler-Bernoulli Beam Using a Complex Variable Semi-Analytical Method," *ASME*, 2009, pp. 375–380.
- [59] Ubessi, C. J. B., and Marczak, R. J., "Sensitivity Analysis of 3D Frictional Contact with BEM Using Complex-Step Differentiation," *Latin American Journal of Solids and Structures*, Vol. 15, No. 10, 2018.  
<https://doi.org/10.1590/1679-78254334>
- [60] Ramirez Tamayo, D., Montoya, A., and Millwater, H., "A Virtual Crack Extension Method for Thermoelastic Fracture Using a Complex-Variable Finite Element Method," *Engineering Fracture Mechanics*, Vol. 192, April 2018, pp. 328–342.  
<https://doi.org/10.1016/j.engfracmech.2017.12.013>
- [61] Montoya, A., Ramirez-Tamayo, D., Millwater, H. R., and Kirby, M., "A Complex-Variable Virtual Crack Extension Finite Element Method for Elastic-Plastic Fracture Mechanics," *Engineering Fracture Mechanics*, Vol. 202, Oct. 2018, pp. 242–258.  
<https://doi.org/10.1016/j.engfracmech.2018.09.023>
- [62] Rincon-Tabares, J.-S., Velasquez-Gonzalez, J. C., Ramirez-Tamayo, D., Montoya, A., Millwater, H., and Restrepo, D., "Sensitivity Analysis for Transient Thermal Problems Using the Complex-Variable Finite Element Method," *Applied Sciences*, Vol. 12, No. 5, 2022, p. 2738.  
<https://doi.org/10.3390/app12052738>
- [63] Gao, X.-W., and He, M.-C., "A New Inverse Analysis Approach for Multi-Region Heat Conduction BEM Using Complex-Variable-Differentiation Method," *Engineering Analysis with Boundary Elements*, Vol. 29, No. 8, 2005, pp. 788–795.  
<https://doi.org/10.1016/jenganabound.2005.03.001>
- [64] Voorhees, A., Millwater, H. R., Bagley, R., and Golden, P., "Fatigue Sensitivity Analysis Using Complex Variable Methods," *International Journal of Fatigue*, Vol. 40, July 2012, pp. 61–73.  
<https://doi.org/10.1016/j.ijfatigue.2012.01.016>
- [65] Montoya, A., Fielder, R., Gomez-Farias, A., and Millwater, H., "Finite-Element Sensitivity for Plasticity Using Complex Variable Methods," *Journal of Engineering Mechanics*, Vol. 141, No. 2, 2015, Paper 04014118.  
[https://doi.org/10.1061/\(ASCE\)EM.1943-7889.0000837](https://doi.org/10.1061/(ASCE)EM.1943-7889.0000837)
- [66] Gomez-Farias, A., Montoya, A., and Millwater, H., "Complex Finite Element Sensitivity Method for Creep Analysis," *International Journal of Pressure Vessels and Piping*, Vols. 132–133, Aug. 2015, pp. 27–42.  
<https://doi.org/10.1016/j.ijpvp.2015.05.006>
- [67] Monsalvo, J. F., García, M. J., Millwater, H. R., and Feng, Y., "Sensitivity Analysis for Radiofrequency Induced Thermal Therapies Using the Complex Finite Element Method," *Finite Elements in Analysis and Design*, Vol. 135, Nov. 2017, pp. 11–21.  
<https://doi.org/10.1016/j.finel.2017.07.001>
- [68] Fielder, R., Montoya, A., Millwater, H., and Golden, P., "Residual Stress Sensitivity Analysis Using a Complex Variable Finite Element Method," *International Journal of Mechanical Sciences*, Vol. 133, Aug. 2017, pp. 112–120.  
<https://doi.org/10.1016/j.ijmecsci.2017.08.035>
- [69] Wagner, D., Garcia, M. J., Montoya, A., and Millwater, H. R., "A Finite Element-Based Adaptive Energy Response Function Method for 2D Curvilinear Progressive Fracture," *International Journal of Fatigue*, Vol. 127, Nov. 2018, pp. 229–245.  
<https://doi.org/10.1016/j.ijfatigue.2019.05.036>
- [70] Pozrikidis, C., *Introduction to Finite and Spectral Element Methods Using Matlab*, CRC Press, Boca Raton, FL, 2005, pp. 23–25.
- [71] Bathe, K.-J., *Finite Element Procedures*, Prentice-Hall, Englewood Cliffs, NJ, 1996, pp. 768–774.
- [72] De Basabe, J. D., and Sen, M. K., "New Developments in the Finite Element Method for Seismic Modeling," *Leading Edge*, Vol. 28, No. 5, 2009, pp. 562–567.
- [73] Kudela, P., Krawczuk, M., and Ostachowicz, W., "Wave Propagation Modelling in 1D Structures Using Spectral Finite Elements," *Journal of Sound and Vibration*, Vol. 300, Nos. 1–2, 2007, pp. 88–100.  
<https://doi.org/10.1016/j.jsv.2006.07.031>
- [74] Komatitsch, D., and Tromp, J., "Introduction to the Spectral Element Method for Three-Dimensional Seismic Wave Propagation," *Geophysical Journal International*, Vol. 139, No. 3, 1999, pp. 806–822.  
<https://doi.org/10.1046/j.1365-246x.1999.00967.x>
- [75] Willberg, C., Duczek, S., Vivar Perez, J. M., Schmicker, D., and Gabbert, U., "Comparison of Different Higher Order Finite Element Schemes for the Simulation of Lamb Waves," *Computer Methods in Applied Mechanics and Engineering*, Vols. 241–244, Oct. 2012, pp. 246–261.  
<https://doi.org/10.1016/j.cma.2012.06.011>
- [76] Mitra, M., and Gopalakrishnan, S., "Guided Wave Based Structural Health Monitoring: A Review," *Smart Materials and Structures*, Vol. 25, No. 5, 2016, Paper 053001.  
<https://doi.org/10.1088/0964-1726/25/5/053001>
- [77] Witkowski, W., Rucka, M., Chróścielewski, J., and Wilde, K., "On Some Properties of 2D Spectral Finite Elements in Problems of Wave Propagation," *Finite Elements in Analysis and Design*, Vol. 55, Aug. 2012, pp. 31–41.  
<https://doi.org/10.1016/j.finel.2012.02.001>
- [78] Ostachowicz, W., Kudela, P., Krawczuk, M., and Zak, A., *Guided Waves in Structures for SHM*, Wiley, Hoboken, NJ, 2012, pp. 47–92.
- [79] MacLagan-Wedderburn, J. H., "Note on Hypercomplex Numbers," *Proceedings of the Edinburgh Mathematical Society*, Vol. 25, Feb. 1906, pp. 2–4.  
<https://doi.org/10.1017/S0013091500033460>
- [80] Baley Price, G., *An Introduction to Multicomplex Spaces and Functions*, Dekker, New York, 1991, pp. 322–371.
- [81] Hamilton, W. R., "XI. On Quaternions; Or on a New System of Imaginaries in Algebra," *London, Edinburgh, and Dublin Philosophical Magazine and Journal of Science*, Vol. 33, No. 219, 1848, pp. 58–60.  
<https://doi.org/10.1080/14786444808646046>
- [82] Millwater, H. R., and Shirinkam, S., "Multicomplex Taylor Series Expansion for Computing High-Order Derivatives," *International Journal of Applied Mathematics*, Vol. 27, No. 4, 2014, pp. 495–502.  
<https://doi.org/10.12732/ijam.v27i4.2>
- [83] Aguirre-Mesa, A. M., Garcia, M. J., and Millwater, H. R., "MultiZ: A Library for Computation of High Order Derivatives Using Multicomplex or Multitudinal Numbers," *ACM Transactions on Mathematical Software*, Vol. 46, No. 3, 2020, pp. 1–30.  
<https://doi.org/10.1145/3378538>
- [84] Aguirre-Mesa, A. M., Garcia, M. J., Aristizabal, M., Wagner, D., Ramirez-Tamayo, D., Montoya, A., and Millwater, H., "A Block Forward Substitution Method for Solving the Hypercomplex Finite Element System of Equations," *Computer Methods in Applied Mechanics and Engineering*, Vol. 387, Dec. 2021, Paper 114195.  
<https://doi.org/10.1016/j.cma.2021.114195>
- [85] Dunham, B. Z., "High-Order Automatic Differentiation of Unmodified Linear Algebra Routines via Nilpotent Matrices," Doctoral Dissertation, Univ. of Colorado, Boulder, CO, 2017.
- [86] Imoto, Y., Yamanaka, N., Uramoto, T., Tanaka, M., Fujikawa, M., and Mitsume, N., "Fundamental Theorem of Matrix Representations of Hyper-Dual Numbers for Computing Higher-Order Derivatives,"

- JSIAM Letters*, Vol. 12, 2020, pp. 29–32.  
<https://doi.org/10.14495/jsiaml.12.29>
- [87] Varas Casado, J., and Hewson, R., “Multicomplex Number Class for Matlab, with a Focus on the Accurate Calculation of Small Imaginary Terms for Multicomplex Step Sensitivity Calculations,” *ACM Transactions on Mathematical Software*, Vol. 46, No. 2, 2020, pp. 1–26.
- [88] Kantor, I. L., and Solodovnikov, A. S. S., “Hypercomplex Numbers,” *Hypercomplex Numbers*, Springer, New York, 1989, pp. 35–39.
- [89] Noh, G., and Bathe, K.-J., “An Explicit Time Integration Scheme for the Analysis of Wave Propagations,” *Computers & Structures*, Vol. 129, Dec. 2013, pp. 178–193.  
<https://doi.org/10.1016/j.compstruc.2013.06.007>
- [90] Zakian, P., and Bathe, K.-J., “Transient Wave Propagations with the Noh-Bathe Scheme and the Spectral Element Method,” *Computers & Structures*, Vol. 254, Oct. 2021, Paper 106531.  
<https://doi.org/10.1016/j.compstruc.2021.106531>
- [91] Millwater, H. R., Wagner, D., Garza, J. E., Baines, A., and Lovelady, K., “Application of the Complex Variable Finite Element Method, ZFEM, to Structural Mechanics Sensitivity Analysis,” *54th AIAA/ASME/ASCE/AHS/ASC Structures, Structural Dynamics, and Materials Conference*, AIAA Paper 2013-1579, 2013.
- [92] Millwater, H., Wagner, D., Baines, A., and Lovelady, K., “Improved WCTSE Method for the Generation of 2D Weight Functions Through Implementation into a Commercial Finite Element Code,” *Engineering Fracture Mechanics*, Vol. 109, Sept. 2013, pp. 302–309.  
<https://doi.org/10.1016/j.engfracmech.2013.07.012>
- [93] Zakian, P., and Khaji, N., “A Novel Stochastic-Spectral Finite Element Method for Analysis of Elastodynamic Problems in the Time Domain,” *Meccanica*, Vol. 51, No. 4, 2016, pp. 893–920.  
<https://doi.org/10.1007/s11012-015-0242-9>
- [94] Zakian, P., Khaji, N., and Kaveh, A., “Graph Theoretical Methods for Efficient Stochastic Finite Element Analysis of Structures,” *Computers & Structures*, Vol. 178, Jan. 2017, pp. 29–46.  
<https://doi.org/10.1016/j.compstruc.2016.10.009>
- [95] Rao, S. S., *Vibration of Continuous Systems*, Wiley, Hoboken, NJ, 2006, pp. 234–256.
- [96] Han, L., Wang, J., Li, H., and Sun, G., “A Time-Domain Spectral Element Method with C1 Continuity for Static and Dynamic Analysis of Frame Structures,” *Structures*, Vol. 28, March 2020, pp. 604–613.  
<https://doi.org/10.1016/j.istruc.2020.08.074>
- [97] Kapuria, S., and Jain, M., “A C1-Continuous Time Domain Spectral Finite Element for Wave Propagation Analysis of Euler–Bernoulli Beams,” *International Journal for Numerical Methods in Engineering*, Vol. 122, No. 11, 2021, pp. 2631–2652.  
<https://doi.org/10.1002/nme.6612>
- [98] Jain, M., and Kapuria, S., “Time-Domain Spectral Finite Element Based on Third-Order Theory for Efficient Modelling of Guided Wave Propagation in Beams and Panels,” *Acta Mechanica*, Vol. 233, No. 3, 2022, pp. 1187–1212.  
<https://doi.org/10.1007/s00707-021-03133-y>

W. Yu  
 Associate Editor